Master Mécanique, Energétique et Ingénieries DE GRENOBLE

Master Geomechanics, Civil Engineering and Risks

Homogenization of a Cracked Poroelastic Medium - Numerical calculation of the coefficients and damage

Albert Argilaga Claramunt

Thesis

Presented in partial fulfilment of the requirements for the degree of

Master Mécanique, Energétique et Ingénieries

Spécialité internationale "Géomécanique, Génie Civil et Risques"

(Geomechanics, Civil Engineering and Risks)

Université Joseph Fourier – Grenoble INP

June, 2013

Project Advisor(s):

- Denis Caillerie, Professor of Grenoble INP
- Stefano Dal Pont, Professor of Grenoble-UJF
- Ferdinando Marinelli, Post doctorant student of Grenoble INP

UNIVERSITE JOSEPH FOURIER
SCIENCES.TECHNOLOGIE.SANTÉ

Grenoble INP

Abstract

This work is devoted to the use of double scale asymptotic expansions and the posterior use of numerical tools in order to get the coefficients for an homogeneous macroscopic model starting from heterogeneous microscopic description. The particular problem of this project is a cracked poroelastic medium, that is a Biot-type problem both in the grains and in the cracks. In order to solve the expanded problem resulting from the double scale asymptotic expansions a finite element code is used. Numerical simulations allow one to obtain the homogenized coefficients for a macroscale description. These results are not isotropic despite having isotropic microscale coefficients due to the crack geometry and orientation. In a second part of the project damage is introduced in the cracks. Damage depends on the crack's opening, this makes the problem nonlinear and makes necessary the use of appropriate numerical tools to find the solution. The commercial finite element code used in the first part can not reproduce the damage problem, therefore a Matlab code is developed. This code consists of a FEM implementation in the porous part, with the appropriate linking conditions for the cracks to create the macrograin in the REV. In order to find the solution for the different nonlinearities of the problem iterative procedures such as the secant method are introduced. The resulting model is able to reproduce any time-history of strain, and an evolution of the homogenized coefficients can be obtained from this time-history, unlike in the linear case, bifurcation phenomena can be observed for the damage problem.

Contents

Introduction

The micro-structure of a material can sometimes be crucial for a macroscopic problem and its influence should be studied. A characteristic example would be the study of the influence of a fissure/crack network on the mechanical and flow properties of a rock mass. The two main approaches that can be followed are continuum mechanics and discrete mechanics. This thesis refers to the determination of the overall poroelastic properties of saturated, cracked, deformable porous medium in the framework of small strains, following a continuum mechanics approach.

The method used for the determination of these overall poroelastic properties is numerical, more specifically the finite element method. Because the result of the double scale asymptotic expansions are two uncoupled boundary value problems (one purely mechanic and another purely hydraulic) it is possible to solve independently both problems in order to get the homogenized coefficients for the elasticity, Biot and permeability problems. Due to the linearity of this problem any unitary macroscale strain value can be applied to the different degrees of freedom in order to obtain the coefficients.

In the second part of this project damage is introduced in the cracks. Damage depends on the opening of the cracks, it is shown that it makes the problem nonlinear. To define the damage, a dimensionless parameter is introduced. This parameter defines the degradation of the cracks from 0 to 1, 0 means no opening and no degradation of the elastic or hydraulic properties, 1 means no contact between the crack lips, and consequently total degradation of the elastic and hydraulic properties. A constitutive law relates the damage parameter and the degradation of the mentioned coefficients. In order to solve this problem numerically, the macroscale strain must be applied using a stepping (iterative method) due to the uncertainty on the damage evolution (is not known whether the crack is opening or not before the calculation of each step) and each step must be solved using again some iterative method due to the nonlinearity coming from the constitutive law.

Chapter 1

Micro-structure and microscopic description

1.1 Description of the crack problem

Cracks are considered as thin layers of a porous medium which has high permeability and very low stiffness with respect to the main porous medium. The idea is to represent cracks as a one-dimensional medium with a form of pillars (Figure 1.1).

1.2 Governing Equations

The porous matrix is considered as a poroelastic material. The deformation and flow in it are governed by Biot's equations of poroelasticity. The problem on each REV[1] of the body is described by the following governing equations[2]:

1.2.1 For the porous part:

- Linear Momentum Balance (LMB)

$$div(\sigma) = 0 \tag{1.1}$$

- Biot Constitutive Equation

$$\sigma = \mathbb{C}@\epsilon(\overrightarrow{u}) - p\alpha \tag{1.2}$$

- Variation of Porosity

$$\delta\eta = (\gamma - \eta_0\mathbb{I}) : \epsilon(\overrightarrow{u}) + \beta p \tag{1.3}$$

- Fluid Volume Balance

$$div(\eta_0(\overrightarrow{v}^{pf} - \dot{\overrightarrow{u}})) + \delta\dot{\eta} + \eta_0 div(\dot{\overrightarrow{u}}) = 0 \tag{1.4}$$

[1] Representative Elementary Volume.

[2] Small strain approximation is taken into account, so $\epsilon = \frac{1}{2}\left(\nabla\vec{u}^t + \nabla\overrightarrow{u}\right)$ this definition makes the strain tensor symmetric $\epsilon = \epsilon^t$

- Darcy Fluid Constitutive Equation

$$\eta_0(\overrightarrow{v}^{pf} - \dot{\overrightarrow{u}}) = -K@\overrightarrow{\nabla}(p) \tag{1.5}$$

1.2.2 For the cracks/interfaces

Here a new curvilinear space variable s along the crack and the tangential unit vector along the crack $\overrightarrow{\tau}$ are introduced. The double brackets [[.]] symbolize a jump of a variable through the crack.

- Darcy fluid constitutive equation

$$Q = -k(\overrightarrow{\nabla}p.\overrightarrow{\tau}) \tag{1.6}$$

- Fluid volume balance

$$[[\eta_{0(nm)}(\overrightarrow{v}^{pf} - \dot{\overrightarrow{u}}_{(nm)})]].n_{(nm)} + \frac{dQ_{(nm)}}{ds} = -A.[[\dot{\overrightarrow{u}}]] - B\dot{p} \tag{1.7}$$

- Continuity of stress

$$[[\sigma@\overrightarrow{n}]] = 0 \tag{1.8}$$

- Biot-type Constitutive equation

$$\sigma@\overrightarrow{n} = D@[[\overrightarrow{u}]] - pA \tag{1.9}$$

In the following, the relative flow vector of the fluid volume $\eta_{0(nm)}(\overrightarrow{v}^{pf(e)} - \dot{\overrightarrow{u}}^{(e)}_{(nm)})$ is denoted by $\overrightarrow{q}$.

1.3 Volume balance at nodes

In order to obtain the volumetric flux balance on each node for an arbitrary crack network, let's denote a topology table that contains the origin "O" and extremity "E" nodes of each crack. The origin nodes give negative flux while the extremity nodes give positive flux.

$$\sum_{b \in E^{-1(n)}} Q^{(b)} - \sum_{b \in O^{-1(n)}} Q^{(b)} + Q^{e/n} = 0 \tag{1.10}$$

The orientation of the cracks is presented in the domain Ω (Figure 1.1). The sub-domains of the REV are denoted by $\prod_n$, n = 1, 2, 3, 4 and the cracks by $\Gamma_{(nm)}$ where n is the number of the sub-domain, to which the normal vector of the crack is inward and m the number of the other. N1 and N2 are denoted the extremity and origin nodes of crack Γ_{14}. N_1 is an external node while N_2 an internal because of their position.

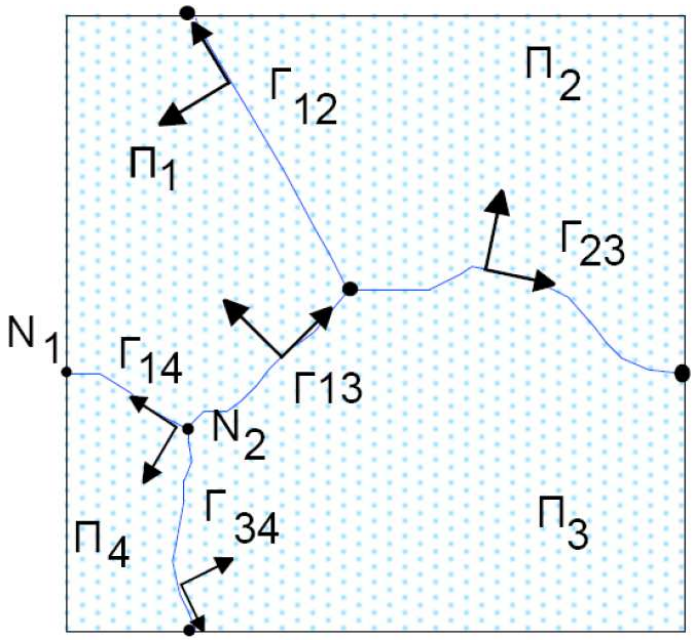

Figure 1.1: Domain Ω. Sub-domains, crack orientation, origin and extremity nodes of a crack.

Chapter 2

Homogenization

The porous part is assumed to be homogeneous and the cracks to be periodically distributed, with a period eY (Figure 2.1), where e is the separation of scales. The size of the period is supposed to be very small with respect to the sample. In the following Y denotes the unit cell (REV) Y^{Γ} the cracks and Yp the porous part in the cell.

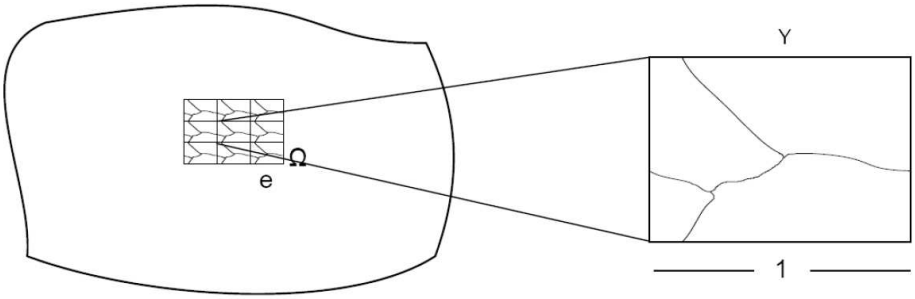

Figure 2.1: Periodic medium and unit cell

2.1 Asymptotic expansions, building the BVP in the REV

The governing equations of the previous section are rewritten taking into account the separation of scales (Caillerie, 2009)[1]. For the specific problem, the primary variables are considered to be the displacement $\overrightarrow{u}$ and the pressure p. We look for the solution of the problem in the form of double scale expansions $\vec{u}^{(e)}$ and $p^{(e)}$.

The primary variables are expanded in the following form :

$$\overrightarrow{u}^{(e)} = \overrightarrow{u}^{(0)}(\overrightarrow{x}) + e\,\overrightarrow{u}^{(1)}(\overrightarrow{x}, \frac{\overrightarrow{x}}{e}) + e^2\overrightarrow{u}^{(2)}(\overrightarrow{x}, \frac{\overrightarrow{x}}{e}) + ... \tag{2.1}$$

$$p^{(e)} = p^{(0)}(\overrightarrow{x}) + ep^{(1)}(\overrightarrow{x}, \frac{\overrightarrow{x}}{e}) + e^2p^{(2)}(\overrightarrow{x}, \frac{\overrightarrow{x}}{e}) + ... \tag{2.2}$$

Only the first term of the series are taken into account for this study.

The expansions of the secondary variables come from the use of the primary ones in any sort of constitutive relation. Each term is a function of the two space variables x and y, where $y = \frac{x}{e}$. Using the chain rule for a function $\phi(x, y)$ the spatial derivative is given by:

$$\frac{d(.)}{d\overrightarrow{X}} = \frac{\partial(.)}{\partial\vec{x}} + \frac{1}{e}\frac{\partial(.)}{\partial\overrightarrow{y}} \tag{2.3}$$

Gathering all the expanding equations derived from the above expressions we obtain the expanded problem, this problem splits in different orders of e, building BVP in REV (Papachristos, 2012)[3].

2.1.1 BVP of $u^{(1)}$on the unit cell

Considering the problem of $u^{(0)}$ and $p^{(0)}$ to be known, these two variables are taken as data for the problem of $u^{(1)}$. The equations that describe this problem are the following:

$$BVP(I)\begin{cases} div^y(\sigma^{(0)}) = 0 & in\, Y \\ \sigma^{(0)} = \mathbb{C}@(\epsilon^x(\overrightarrow{u}^{(0)}) + \epsilon^y(\overrightarrow{u}^{(1)})) - \alpha p^{(0)} & in\, Y^p \\ [[\overrightarrow{t}^{(0)}]] = 0 & on\, c \\ \overrightarrow{t}^{(0)} = D@[[\overrightarrow{u}^{(1)}(\overrightarrow{x}, \overrightarrow{y})]] - \overrightarrow{A}p^{(0)}(\overrightarrow{x}) & on\, c \\ +periodicity\, of\, u^{(1)} & in\, Y \end{cases} \tag{2.4}$$

2.1.2 BVP of $p^{(1)}$on the unit cell

Considering the problem of $u^{(0)}$ and $p^{(0)}$ to be known, these two variables are taken as data for the problem of $p^{(1)}$. The equations that describe this problem are the following[1]:

$$BVP(II)\begin{cases} div(q^{(0)}) = 0 & in\, Y^p \\ [[q^{(0)}]].\overrightarrow{n} + \frac{dQ^{(0)}}{ds} = 0 & in\, Y^\Gamma \\ +Darcy\, expansions & in\, Y \\ +periocity\, of\, \nabla p^{(1)} & in\, Y \end{cases} \tag{2.5}$$

[1] Darcy equation (Eq. 1.5) is used in the microscale description, it can create confusion due to the fact that this is an integrated equation which comes from an homogenization problem, in this project the microscale is represented by the crack network well separated from the macroscale in which the cacks can not be seen. The Darcy description comes from the water flow in the pores in a third and smaller scale already taken into consideration as an integrated equation in the microscale of the present project.

2.2 Macroscopic model: constitutive law

In this section the integrated expressions of the previous boundary value problems are presented, the homogenized coefficients can be obtained from numerical results using these equations.

2.2.1 Linear Momentum Balance

$$div^x \sum^{(0)} = 0 \tag{2.6}$$

$$\mid \mathrm{Y} \mid \sum\nolimits_{ij}^{(0)} = \mathcal{C}_{ijlm} \epsilon_{lm}^x(\vec{u}^{(0)}) - \mathbf{a}_{ij} p^{(0)} \tag{2.7}$$

- Homogenized elastic coefficient

$$\mathcal{C}_{ijlm} = \mathbb{C}_{ijlm} |Y^p| + \int_{Y^p} [\mathbb{C}_{ijkh} \epsilon_{kh}^y(\overrightarrow{\xi_{lm}})] dv^y \tag{2.8}$$

- Homogenized Biot's coefficient

$$\mathbf{a}_{ij} = \int_{Y^p} [\mathbb{C}_{ijkh} \epsilon_{kh}(\overrightarrow{\pi})] dv^y - \alpha_{ij} |Y^p| \tag{2.9}$$

2.2.2 Fluid Volume Balance

$$\overrightarrow{q}^{HOM} + \delta \dot{\Phi} = 0 \tag{2.10}$$

The Darcy law:

$$\overrightarrow{q}^{HOM} = -K^{HOM} @ \nabla^x \vec{p}^{(0)} \tag{2.11}$$

With the homogenized permeability tensor K^{HOM} defined as:

$$K^{HOM} = \int_{Y^p} K \circ (\mathbb{I} + \nabla^y(\vec{\chi})) dv^y + \int_c [(k(\mathbb{I} + \nabla^y(\vec{\chi}))^t @ \vec{\tau}] dl_c \tag{2.12}$$

Chapter 3

Numerical resolution

Since an homogenoeus solution can not be expected numerical tools are needed. In this chapter a commercial finite element software is used in order to find a numerical solution for the two boundary value problems described in the previous part. Classical PDE problem descriptions are used in the numerical implementation[1] adding in each case the macroscale terms as a linear form in the weak expression of the virtual power formulation (Eq. 3.1):

$$\forall \overrightarrow{v}, a(\vec{u}, \overrightarrow{v}) + b(\overrightarrow{R}, \overrightarrow{v}) = L(\overrightarrow{v}) \tag{3.1}$$

$a(\vec{u}, \overrightarrow{v})$ symmetrical bilinear form
$b(\overrightarrow{R}, \overrightarrow{v})$ non symmetrical bilinear form with respect to $\overrightarrow{R}$ and $\vec{v}$
$L(\overrightarrow{v})$ linear form (in the present problem macroscale terms)

A REV of a given crack geometry (Figure 3.1) is considered in order to apply the numerical model.

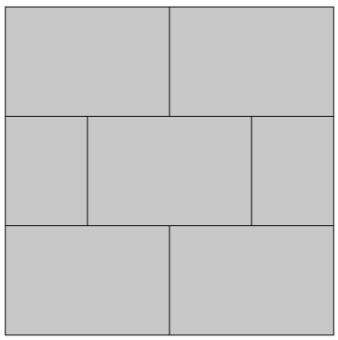

Figure 3.1: Crack geometry in a REV (Marinelli, 2013)[2].

[1] In particular the prototypical parabolic partial differential equation for the hydraulic problem and the elliptic one for the mechanical.

3.1 Mechanical problem

3.1.1 Validation

In order to validate the numerical model, a simulation of a one dimensional simple configuration with one single vertical crack and a macroscopic strain applied to the axis orthogonal to this crack is carried. As it is possible to prove that the solution is homogeneous in the grains (sub-domains inside Ω), and the stress derivatives with respect the direction of the crack are 0 (Eq. 3.8 and 3.9), we can easily find the analytical solution to this problem (Eq. 3.16). The procedure is described and the numerical analogous calculation (Figure 3.2) presented in the following :

BVP (I):

$$div^y(\sigma^{(0)}) = 0 \tag{3.2}$$

$$\sigma^{(0)} = \mathbb{C}@(\epsilon^x(\overrightarrow{u}^{(0)}) + \epsilon^y(\overrightarrow{u}^{(1)})) - \alpha p^{(0)} \tag{3.3}$$

$$[[\overrightarrow{t}^{(0)}]] = 0 \tag{3.4}$$

$$\overrightarrow{t}^{(0)} = D@[[\overrightarrow{u}^{(1)}(\overrightarrow{x}, \overrightarrow{y})]] - \overrightarrow{A}p^{(0)}(\overrightarrow{x}) \tag{3.5}$$

$$+periodicity\, of\, u^{(1)} on\, the\, unit\, cell \tag{3.6}$$

For this case D is assumed to be a diagonal matrix defined as:

$$D = k\begin{pmatrix} 1 & 0 \\ 0 & 1 \end{pmatrix} \tag{3.7}$$

We look for a solution depending on y_1 only

$$\frac{\partial \sigma_{11}}{\partial y_2} = 0 \tag{3.8}$$

and

$$\frac{\partial \sigma_{12}}{\partial y_2} = 0 \tag{3.9}$$

We end up with the following equations to solve:

$$\sigma_{11} = (\lambda + 2\mu)(\varepsilon^x_{11} + \frac{\partial u_1^{(1)}}{\partial y_1}) + \lambda \varepsilon^x_{22} \tag{3.10}$$

$$\sigma_{12} = 2\mu(\varepsilon^x_{12} + \frac{\partial u_2^{(1)}}{\partial y_1}) \tag{3.11}$$

$$\sigma_{22} = \lambda(\varepsilon^x_{11} + \frac{\partial u_1^{(1)}}{\partial y_1}) \tag{3.12}$$

Integrating over L:

$$\sigma_{11} L = (\lambda + 2\mu)(L_1 + L_2)\varepsilon^x_{11} - \lambda[[u_1^{(1)}]]_0^{L_1+L_2} + \lambda(L_1 + L_2)\varepsilon^x_{22} \tag{3.13}$$

$$\sigma_{12}L = 2\mu(L_1 + L_2)\varepsilon^x_{12} - \mu[[u^{(1)}_2]]^{L_1+L_2}_0 \tag{3.14}$$

$$\sigma_{22}L = \lambda(L_1 + L_2)\varepsilon^x_{11} - (\lambda + 2\mu)[[u^{(1)}_1]]^{L_1+L_2}_0 \tag{3.15}$$

For the Lamé constants[2], spring constant per unit area in the crack and applied macro-strain :

$\lambda = 1442 \cdot 10^6 Pa$, $\mu = 961 \cdot 10^6 Pa$, $k = 1 \cdot 10^{12} N/mm^2$ and $\overrightarrow{\varepsilon}^x = (1; 0; 0)$

The following result is obtained for the coefficients of the elasticity matrix:

$$\overrightarrow{C}^H_{11Analytical} = (1,25 \cdot 10^9;\ 5,38 \cdot 10^8;\ 0) \tag{3.16}$$

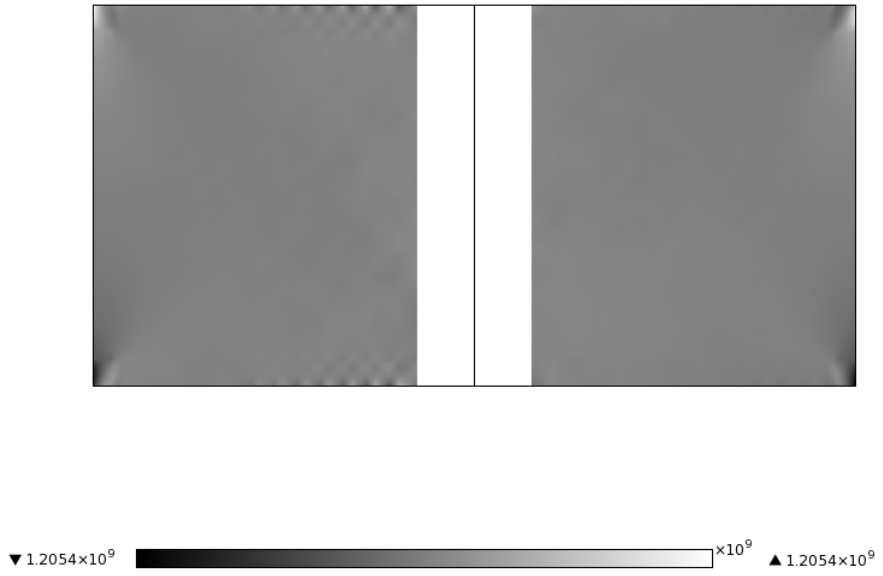

Figure 3.2: Numerical result: plot of the micro-scale Von Misses stress field.

$$\overrightarrow{C}^H_{11Numerical} = (1,25 \cdot 10^9;\ 5,38 \cdot 10^8;\ 0) \tag{3.17}$$

We assume that the validation of the numerical model is successful for the BVP I: $\overrightarrow{C}^H_{11Numerical} = \overrightarrow{C}^H_{11Analytical}$

[2]The Lamé constants are chosen according to the values used in a previous work (Marinelli, 2013)[2] and correspond to a clayrock material. The crack elastic constant value is chosen in order to have a similar contribution to the deformation than the one from the grains. (Range: $1 \cdot 10^9 Pa$ -$1 \cdot 10^{15} Pa$) Lower values will make the behavior of the system only dependent on the crack stiffness, higher values will be equivalent to the non crack problem.

3.1.2 Homogenized coefficients

In this subsection, an REV of the given crack geometry (Figure 3.1) will be numerically solved with given coefficients in the microscale description in order to get the homogenized elasticity and Biot coefficients in the macroscale.

The unknown in the numerical simulation is the micro-scale displacement field. In order to obtain the coefficients, it is needed to integrate[3] this microscale numerical solution (Figure 3.3, 3.4 and 3.5).

The porous medium of the grains is assumed to be homogeneous and isotropic with Lamé constants: $\lambda = 1442 \cdot 10^6 Pa$, $\mu = 961 \cdot 10^6 Pa$

Applied homogenized coefficients: $\overrightarrow{\varepsilon}^x = (\varepsilon_{11};\ \varepsilon_{22};\ \varepsilon_{12})$,[4] $p = 0$, $\alpha = 0$ **and** $\overrightarrow{A} = 0\mathbb{I}$ In the following results, coefficients are presented for a different values of the spring constant in the thin elastic layer:

No cracks[5]

$$\overrightarrow{S}^H = \begin{pmatrix} 3,36 \cdot 10^9 & 1,44 \cdot 10^9 & 0 \\ 1,44 \cdot 10^9 & 3,36 \cdot 10^9 & 0 \\ 0 & 0 & 1,92 \cdot 10^9 \end{pmatrix} = \begin{pmatrix} \lambda + 2\mu & \lambda & 0 \\ \lambda & \lambda + 2\mu & 0 \\ 0 & 0 & 2\mu \end{pmatrix} \tag{3.18}$$

Thin elastic layer spring constant per unit area: $1 \cdot 10^{12} Pa$ (Figure3.3)

$$\overrightarrow{S}^H = \begin{pmatrix} 7,48 \cdot 10^8 & 4,93 \cdot 10^7 & 0 \\ 4,93 \cdot 10^7 & 4,26 \cdot 10^8 & 0 \\ 0 & 0 & 4,88 \cdot 10^8 \end{pmatrix} \tag{3.19}$$

Thin elastic layer spring constant per unit area: $1 \cdot 10^9 Pa$ [N/mm2]

$$\overrightarrow{S}^H = \begin{pmatrix} 1,08 \cdot 10^6 & 84,5 & 0 \\ 84,5 & 0,5 \cdot 10^6 & 0 \\ 0 & 0 & 0,658 \cdot 10^5 \end{pmatrix} \tag{3.20}$$

Thin elastic layer spring constant per unit area: $1 \cdot 10^6 Pa$ [N/mm2]

$$\overrightarrow{S}^H = \begin{pmatrix} 1083 & 0 & 0 \\ 0 & 500 & 0 \\ 0 & 0 & 658 \end{pmatrix} \tag{3.21}$$

[3] Using divergence theorem and conservation of momentum the integrated coefficients can be gotten from the average on the boundary of the REV.

[4] Three different macrostrains are applied in order to determine the solution in all the degrees of freedom of the elasticity problem.

[5] Equivalent to very large spring constant in the cracks.

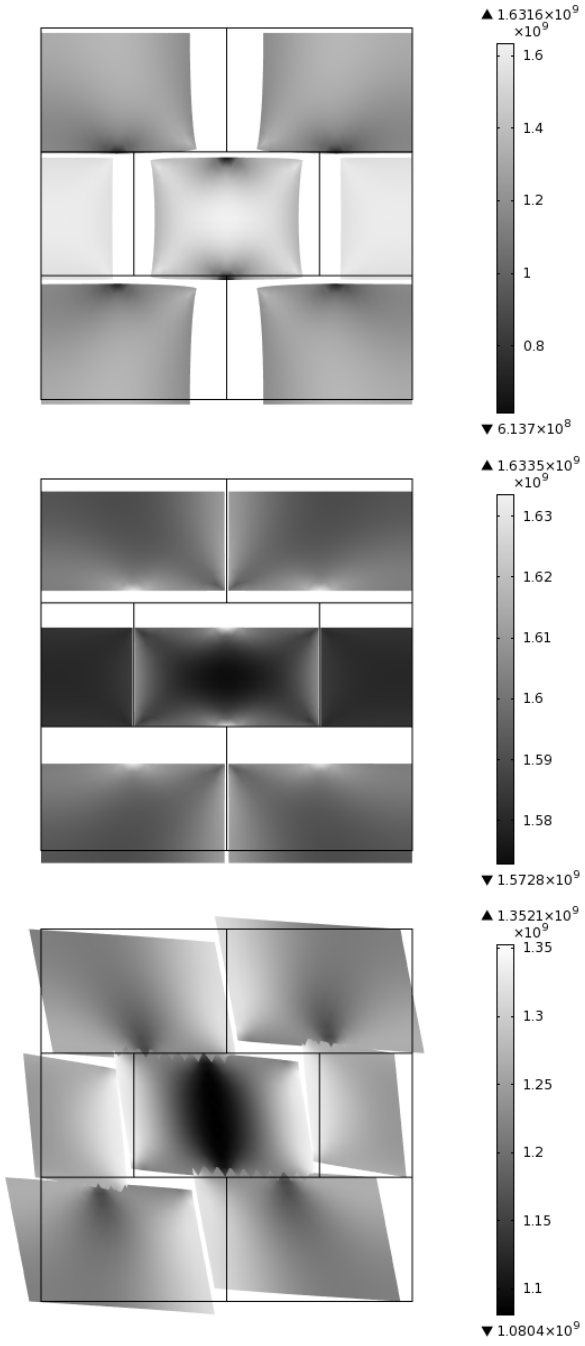

Figure 3.3: Plots of the micro-scale Von Misses stress field [N/mm2]. Thin elastic layer spring constant per unit area: $1 \cdot 10^{12}$ [N/mm2]

Applied homogenized coefficients: $\overrightarrow{\varepsilon}^x = (0;0;0)$**,** $p = 1$**,** $\alpha = 0,4$ **and** $\overrightarrow{A} = X\mathbb{I}$ No cracks[6]

$$\overrightarrow{A}^H = \begin{pmatrix} 0,4 & 0 \\ 0 & 0,4 \end{pmatrix} \tag{3.22}$$

In the following resulting coefficients are presented for different values of the Biot matrix coefficients $\overrightarrow{A}$ in the thin elastic layer, the thin elastic layer spring constant per unit area is set to $1 \cdot 10^{12} Pa$, anyway this parameter has no effect on the calculation for the homogenized Biot coefficients.

$\overrightarrow{A} = 0\mathbb{I}$(Figure3.4)

$$\overrightarrow{A}^H = \begin{pmatrix} -0,3336 & 0 \\ 0 & -0,3604 \end{pmatrix} + \begin{pmatrix} 0,4 & 0 \\ 0 & 0,4 \end{pmatrix} = \begin{pmatrix} 0,0664 & 0 \\ 0 & 0,0396 \end{pmatrix} \tag{3.23}$$

$\overrightarrow{A} = 0,1\mathbb{I}$

$$\overrightarrow{A}^H = \begin{pmatrix} -0,2502 & 0 \\ 0 & -0,2703 \end{pmatrix} + \begin{pmatrix} 0,4 & 0 \\ 0 & 0,4 \end{pmatrix} = \begin{pmatrix} 0,1498 & 0 \\ 0 & 0,1297 \end{pmatrix} \tag{3.24}$$

$\overrightarrow{A} = 0,4\mathbb{I}$

$$\overrightarrow{A}^H = \begin{pmatrix} 0,4 & 0 \\ 0 & 0,4 \end{pmatrix} \tag{3.25}$$

$\overrightarrow{A} = 0,6\mathbb{I}$

$$\overrightarrow{A}^H = \begin{pmatrix} 0.1668 & 0 \\ 0 & 0,1802 \end{pmatrix} + \begin{pmatrix} 0,4 & 0 \\ 0 & 0,4 \end{pmatrix} = \begin{pmatrix} 0,5668 & 0 \\ 0 & 0,5802 \end{pmatrix} \tag{3.26}$$

$\overrightarrow{A} = 1\mathbb{I}$ (Figure3.5)

$$\overrightarrow{A}^H = \begin{pmatrix} 0.5005 & 0 \\ 0 & 0,5406 \end{pmatrix} + \begin{pmatrix} 0,4 & 0 \\ 0 & 0,4 \end{pmatrix} = \begin{pmatrix} 0,9005 & 0 \\ 0 & 0,9406 \end{pmatrix} \tag{3.27}$$

[6] Equivalent to very large spring constant in the cracks.

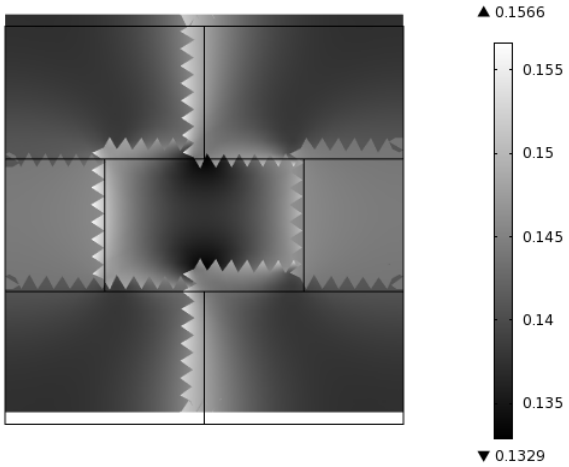

Figure 3.4: Plots of the micro-scale VM stress [N/mm2] for the cases with $\overrightarrow{A} < \vec{\alpha}$. Thin elastic layer any spring constant per unit area: $1 \cdot 10^{12}$ [N/mm2], $\overrightarrow{A} = 0\mathbb{I}$

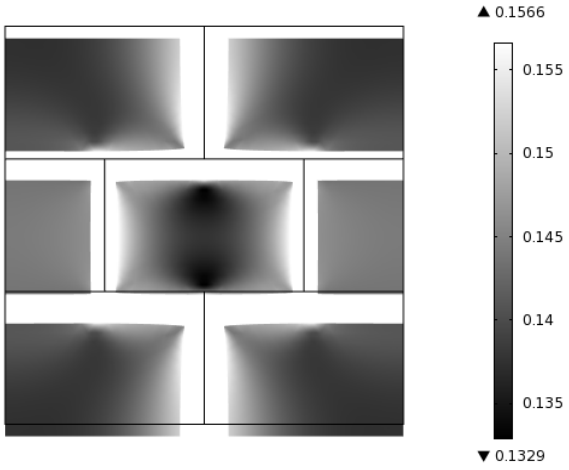

Figure 3.5: Plots of the micro-scale VM stress [N/mm2] for the cases with $\overrightarrow{A} > \vec{\alpha}$. Thin elastic layer any spring constant per unit area: $1 \cdot 10^{12}$ [N/mm2], $\overrightarrow{A} = 1\mathbb{I}$

3.2 Hydraulic problem

3.2.1 Validation

From the definition of the hydraulic problem it is shown that the problem on the cracks and on the grains are independent. Homogeneous solutions for the micro-scale pressure field are obtained for any combination of crack and grain permeability values. Although analytical solution exist, a numerical simulation (Figure 3.6) is carried out for the purpose of validation.

3.2.2 Homogenized coefficients

In this subsection, a REV of the given crack geometry (Figure 3.1) will be numerically solved with given coefficients in the microscale description in order to get the homogenized permeability coefficients in the macroscale.

The porous media of the grains is assumed to be homogeneous and isotropic with diagonal permeability matrix: $k_{11} = k_{22} = 1 \cdot 10^{-10}$m/s and the thin highly permeable layer with $k_{11} = k_{22} = 1 \cdot 10^{-7}$m/s and thickness 0,001 times the cell size.

Applied homogenized coefficients: $\vec{\nabla} p_x^{(0)} = (a, b)$ **(Figure3.6)**

$$\overrightarrow{S}^H = \begin{pmatrix} 2,986 \cdot 10^{-10} & 0 \\ 0 & 2,324 \cdot 10^{-10} \end{pmatrix} \tag{3.28}$$

As the solution is known for this particular problem, we expect a homogeneous pressure field, or in other terms, a constant hydraulic gradient. From the homogenized coefficients it can be said that the coefficient k_{11}^H is higher than k_{22}^H because the crack geometry has more continuous crack paths in this direction than in the other one. It can also be observed that the homogenized coefficients have the expected order of magnitude about 3 times the grain permeability for the x axis and a little bit less for the y axis.

3.3 Discussion of the results

The plots (Figure 3.3, 3.4 and 3.5) present the displacement and stress field[7] in the micro-scale, for the case of no cracks or very stiff cracks, very low values of the displacement are obtained[8]. This can be explained because without cracks all the strain is due the macroscale problem.

Despite having isotropic elasticity, both in the grains and in the cracks, the homogenized solution is not isotropic. This can be put down to the microscale configuration (Figure 3.1). Looking carefully at the resulting homogenized coefficients, it can be seen that in all cases there is a decrease of the resulting stiffness

[7] Von Misses stress: is a scalar stress value proportional to the distortion energy that can be computed from the Cauchy stress tensor. In the principal stresses space can be simplified: $\sigma_v = \sqrt{\frac{1}{2}[(\sigma_1 - \sigma_2)^2 + (\sigma_1 - \sigma_3)^2 + (\sigma_2 - \sigma_3)^2]}$.

[8] Can be considered a numerical zero.

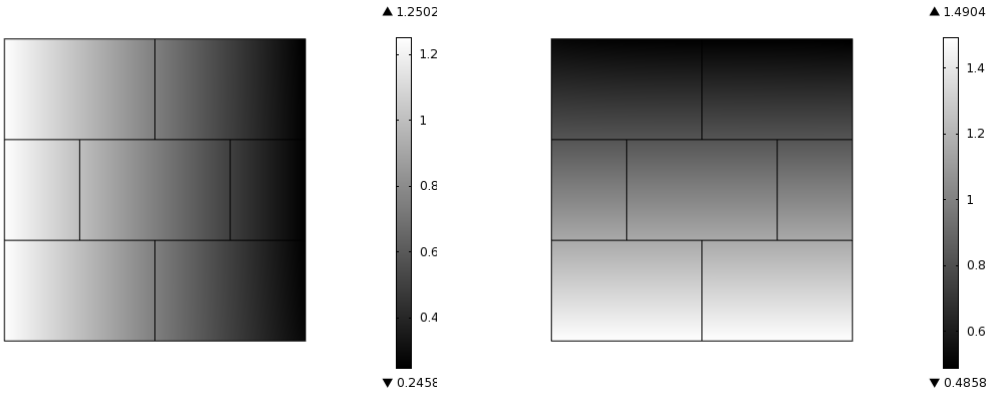

Figure 3.6: Plots of the micro-scale pressure field for the macroscale pressure (1,0) and (0,1)

due to the contribution of the cracks, but if coefficients[9] C_{1111} and C_{2222} are compared, for instance in (Eq. 3.19) it can be seen that C_{1111} is higher than C_{2222}, $7,48 \cdot 10^8$ and $4,26 \cdot 10^8$ respectively. The less stiff behavior in the y axis can be explained because the crack geometry and orientation and the behavior can be observed qualitatively in the stress-deformation plots of the numerical calculation (Figure 3.3). It can also be observed, that the coefficients C_{1112} and C_{2212} are equal to 0, this is because this is an orthotropic case due to the two symmetries in the crack network.

For a low enough crack stiffness a macroscopic behavior independent from the porous part properties can be observed. If the results from (Eq. 3.20 and 3.21) are compared, a linear dependence between the coefficients and the crack stiffness factor can be found. In the other side, if a very stiff crack is considered, the macroscopic behavior will depend only on the porous part properties. This can be observed for values around $1 \cdot 10^{15}$ (Eq. 3.18).

[9] The following Cauchy stress and Biot problem notation is considered:

$$\begin{pmatrix}\sigma_{11}\\ \sigma_{22}\\ \sigma_{12}\end{pmatrix} = \begin{pmatrix}C_{1111} & C_{1122} & C_{1112}\\ C_{1122} & C_{2222} & C_{2212}\\ C_{1112} & C_{2212} & C_{1212}\end{pmatrix}\begin{pmatrix}\epsilon_{11}\\ \epsilon_{22}\\ \epsilon_{12}\end{pmatrix} \text{ and } \overrightarrow{A}^H = \begin{pmatrix}A_{1111} & A_{1212}\\ A_{1212} & A_{2222}\end{pmatrix}$$

Chapter 4

Damage

In the second part of this project, damage is introduced in the cracks. Damage implies a degradation in the elasticity and permeability coefficients of the cracks depending on their opening. This chapter focuses on the study of the nonlinearity. As the nonlinearity comes only from the mechanical problem, the hydraulic problem is not the object of this chapter, the results obtained here can be applied in order to solve a hydraulic problem identical to the one in the previous part (Section 3.2).

4.1 Description of the problem

The description of the homogenized problem is the same as the one in the REV described in the first part of the project (Chapter 2). In the following the added damage state is defined:

A dimensionless parameter $\widehat{\lambda}$ is introduced:

$$\widehat{\lambda} = \sqrt{\left(\frac{\triangle_n}{\delta_n}\right)^2 + \left(\frac{\triangle_t}{\delta_t}\right)^2} \tag{4.1}$$

In the non deformed configuration, because there is no opening in the cracks, $\widehat{\lambda}$ is equal to zero, with the evolving of the opening the damage parameter $\widehat{\lambda}$ increases until it reaches the value 1 when the opening is complete. δ_n and δ_t are considered the critical values respectively for the normal and tangential jump for which the interaction between the two parts becomes zero. For sake of simplicity in the following no difference is made between normal and tangential component of the opening, so the above expression (Eq. 4.1) can be turned into the modulus of the jump divided by the critical value (Eq. 4.2).

$$\widehat{\lambda} = \sqrt{\left(\frac{\triangle_g}{\delta_g}\right)^2} \tag{4.2}$$

A constitutive law is introduced:

$$f(\beta) = \begin{cases} 1 - 2\beta + \beta^2, & 0 \leq \beta 1 < 1 \\ 0 & \beta \geq 1 \end{cases} \tag{4.3}$$

A modified constitutive equation with 1% remaining stiffness is also considered:

$$f_2(\beta) = \begin{cases} 1 - 0,99 \cdot (2\beta - \beta^2), & 0 \leq \beta 1 < 1 \\ 0,01 & \beta \geq 1 \end{cases} \tag{4.4}$$

For a kinematic time-history:

$$t \to \triangle_g(t) \tag{4.5}$$

$\lambda(t)$ is defined as:

$$\lambda(t) = \sup_{\tau \leq t} \hat{\lambda}(\tau) \tag{4.6}$$

Then the constitutive law is defined as:

$$T_t(X) = \frac{1}{\delta_t} f(\lambda(t)) \triangle_n(t) \tag{4.7}$$

Due to these considerations the problem becomes nonlinear. The nonlinearity is due to different mechanisms, one is that a priori we don't know if the damage is going to increase or not. To deal with this the macrostrain should be applied step by step with little increase between steps. In each step the damage will be compared to the previous one in order to set the damage for the next step according to $\lambda(t) = \underset{\tau \leq t}{sup} \hat{\lambda}(\tau)$. But the calculation in each step is still nonlinear due to the constitutive law. This requires an iterative method in order to find the solution in each step of the time-history.

4.2 Numerical model

In order to solve the above problem and taking into account that it is not possible to deal with the nonlinearities with the commercial software used in the first part of this project, a new numerical code must be used. This code is developed using Matlab. First of all a finite element scheme is applied to the two different grain shapes (Figure 4.1) that compose the REV.

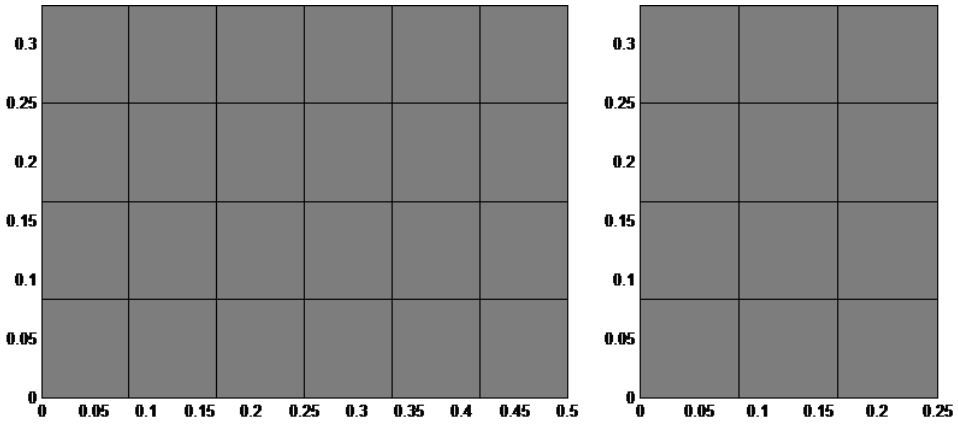

Figure 4.1: Two grain shapes geometry and mesh.

The resulting system matrices are assembled in a global system matrix[1] (Figure 4.2) with the appropriate linking conditions between the different grains. The periodicity conditions are applied using the penalization method and finally one point is fixed using penalization again in order to avoid kinematic indetermination. The size of this system is [430x430][2].

The constitutive equation (Eq.4.3) for the degradation of the elastic properties in the cracks must be implemented in the Gauss points of the discretization. A Gauss-Legendre quadrature is used in order to integrate the function, because the shape functions used in the finite element code are linear functions, from the multiplication of these comes a quadratic function, so two Gauss points in each element are required in order to integrate it exactly. The appropriate Gauss-Legendre positions and weights are used (Figure 4.3).

As mentioned in the previous section, appropriate methods should be used in order to find a solution for the nonlinear problem, the nonlinearity coming from the fact that the damage can only increase is solved using a stepping method and checking the evolution of the damage in each step (Eq. 4.6).

[1] As it is usual in finite element method the system matrix is sparse, this means that it is almost empty with only some of the values different from zero, an optimized strategy to deal with this in Matlab is to preallocate a sparse matrix in order to avoid the use of memory by the zero values.

[2] Note that the dimension of the matrix is twice the number of nodes because the problem is two dimensional, so each of the nodes has two degrees of freedom.

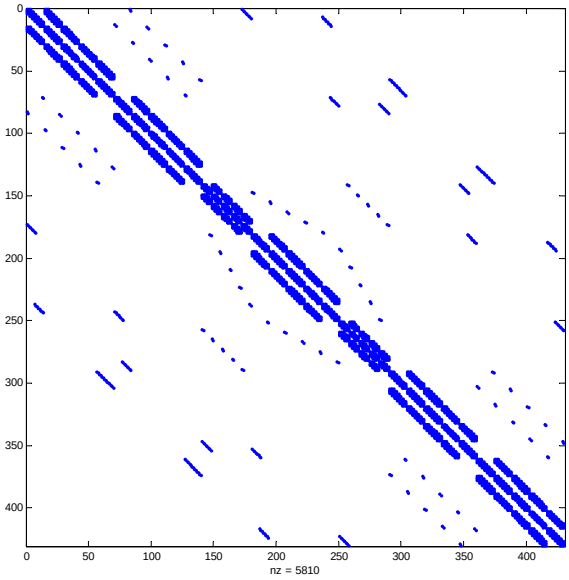

Figure 4.2: Resulting matrix of the assembling, plus crack links and periodicity conditions (penalization method). The positions marked in the plot are the terms different from zero, "nz" is the number of non zero terms, it can be seen that the matrix is sparse, it can also be seen that the shape of the matrix is banded with the coefficients coming from the different grain shapes near the diagonal and further the periodicity and crack links coefficients.

The model is still nonlinear in each iteration due to the constitutive equation (Eq. 4.8). The secant method (Eq. 4.8) will be used in order to find the solution in each iteration. In the following "n" is the iteration number for the secant method[3].

$$x_{n+1} = x_n - \frac{x_n - x_{n-1}}{f(x_n) - f(x_{n-1})} f(x_n) \tag{4.8}$$

[3]The rate of convergence of the secant method near the solution is slower than Newton method: 1,618 against 2, but Newton method requires the evaluation of both the function and derivative in each step or twice the function if finite difference approximation is used, while secant method only requires one evaluation. In the present case, as finite difference approximation is used and parallel computing is not taken into consideration, secant method is faster than Newton method for a given number of steps.

```
for k=1:40[a]
% crack jump on nodes
un1(k)=u(crackga[b](k,1));
un2(k)=u(crackga(k,2));
%crack jump on Gauss points
ugp1(k)=un1(k)*(3^(1/2)/6+0.5)+un2(k)*(-3^(1/2)/6+0.5);
ugp2(k)=un2(k)*(3^(1/2)/6+0.5)+un1(k)*(-3^(1/2)/6+0.5);
end
```

[a] 40 is the number of elements containing at least one lip of the cracks.
[b] List of the nodes corresponding to each element in the FEM implementation.

Figure 4.3: Code for Gauss point evaluation.

```
for i=1:n[a]
macroscale_strain=-0,75*i/n
damgp=max(damgp,damgpi);
f(damgp); %constitutive law
femcode(macroscale_strain,alpha)
damgpi=damgp;
end
```

[a] n is the number of steps in the time-history.

Figure 4.4: Code for time-history stepping for a final macrostrain equal to -0,75

4.3 Results: homogenized coefficient evolution

4.3.1 Time history: xx applied macroscale strain

A macrostrain $\epsilon^x = (\ -0,75 \quad 0 \quad 0\ )$ is applied using the stepping procedure described before. 20 steps are used, the tolerance used to stop the secant method iterations is set to $1 \cdot 10^{-6}$ for the modulus of the vector composed of the incremental jump between iterations on the Gauss points. In the following the resulting values for the homogenized elasticity coefficients are presented for the step 0 (no damage)[4], step 5, step 10, step 15 and step 20 (final state) as well as the plot (Figure 4.6) of the evolution of these values:

$$\overrightarrow{S}^H_{(i=0)} = \begin{pmatrix} 7,48 \cdot 10^8 & 4,93 \cdot 10^7 & 0 \\ 4,93 \cdot 10^7 & 4,26 \cdot 10^8 & 0 \\ 0 & 0 & 4,88 \cdot 10^8 \end{pmatrix} \tag{4.9}$$

$$\overrightarrow{S}^H_{(i=5)} = \begin{pmatrix} 5,87 \cdot 10^8 & 3,53 \cdot 10^7 & 0 \\ 3,53 \cdot 10^7 & 3,92 \cdot 10^8 & 0 \\ 0 & 0 & 4,27 \cdot 10^8 \end{pmatrix} \tag{4.10}$$

$$\overrightarrow{S}^H_{(i=10)} = \begin{pmatrix} 3,52 \cdot 10^8 & 1,79 \cdot 10^7 & 0 \\ 1,79 \cdot 10^7 & 3,46 \cdot 10^8 & 0 \\ 0 & 0 & 3,17 \cdot 10^8 \end{pmatrix} \tag{4.11}$$

$$\overrightarrow{S}^H_{(i=15)} = \begin{pmatrix} 2,73 \cdot 10^7 & 1,01 \cdot 10^6 & 0 \\ 1,01 \cdot 10^6 & 2,65 \cdot 10^8 & 0 \\ 0 & 0 & 4,63e^7 \end{pmatrix} \tag{4.12}$$

$$\overrightarrow{S}^H_{(i=20)} = \begin{pmatrix} 0 & 0 & 0 \\ 0 & 2,61 \cdot 10^8 & 0 \\ 0 & 0 & 0 \end{pmatrix} \tag{4.13}$$

[4] If (Eq. 4.9) is compared with the results of (Eq. 3.19) it can be seen that the values of $\vec{S}^H$ are identical to the ones for the no damage situation (step i=0).

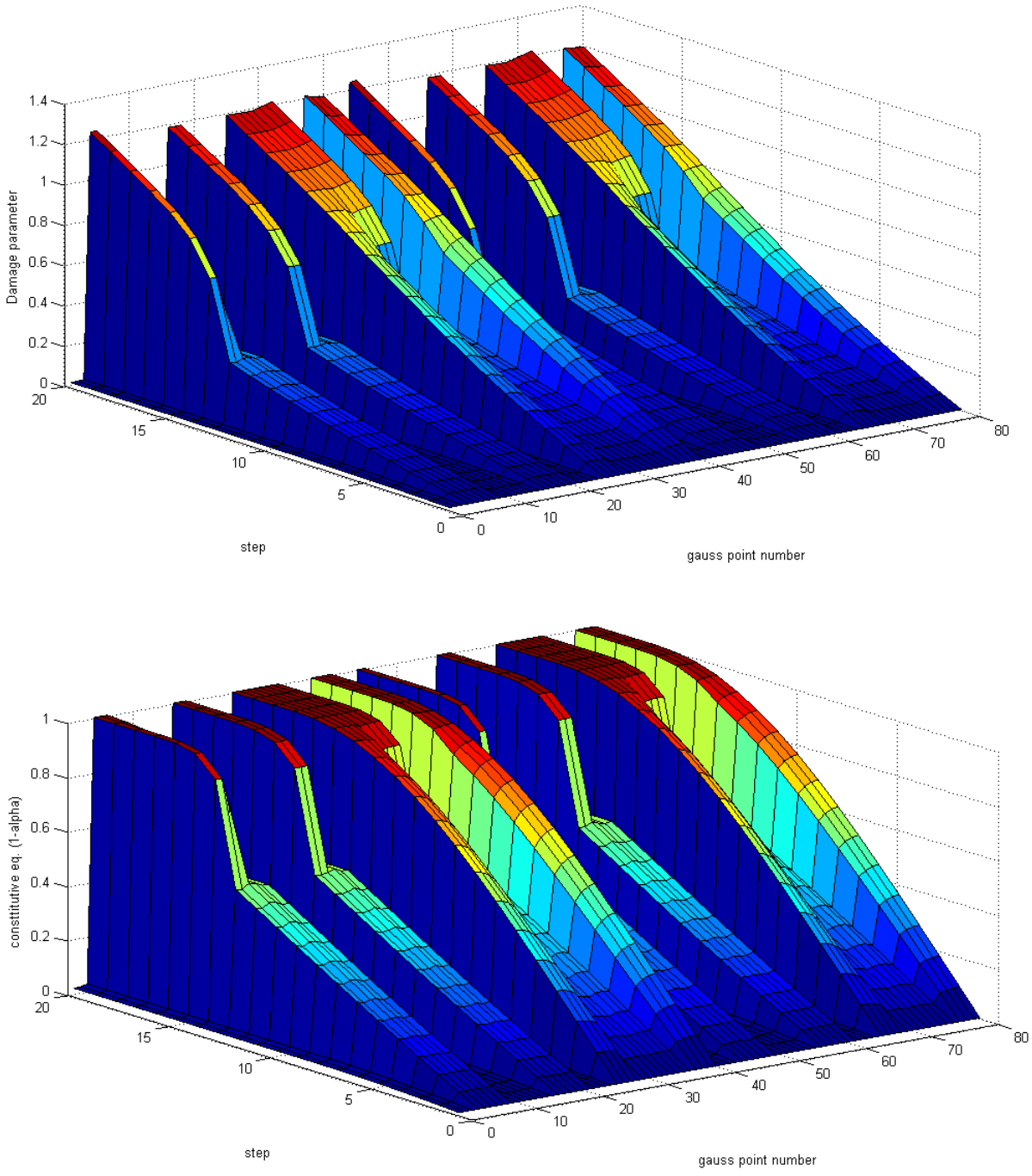

Figure 4.5: Evolution of the damage parameter and constitutive law for all the Gauss points (numbered from 0 to 80). xx applied time history.

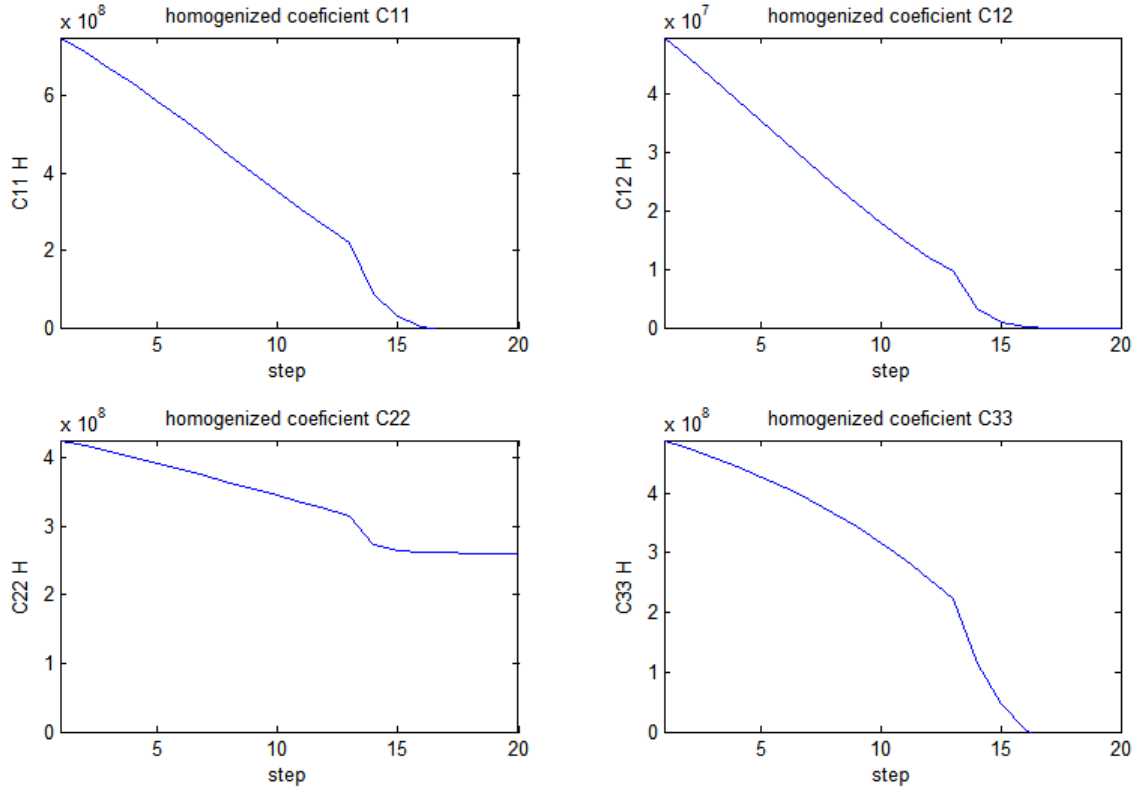

Figure 4.6: Evolution of the homogenized coefficients for the xx applied time history

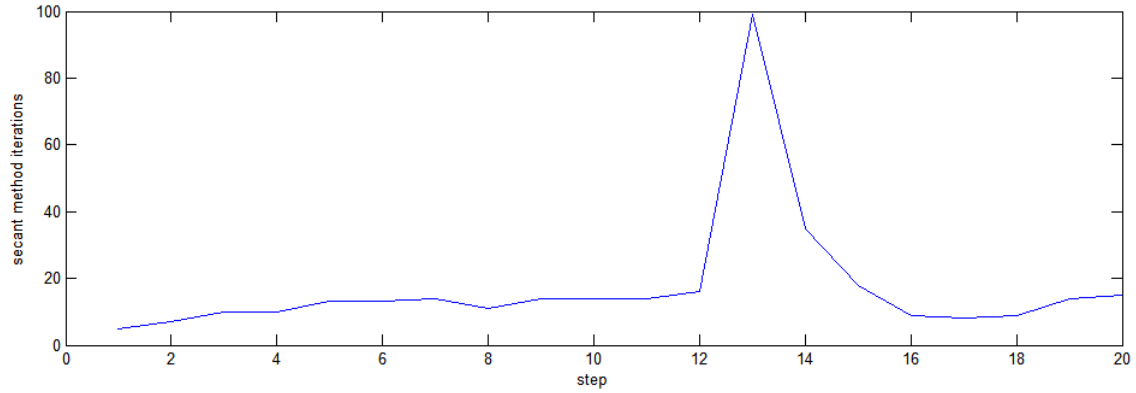

Figure 4.7: Evolution of the number of iteration in the secant method needed to reach the convergence criteria in each step. xx applied time history.

4.3.2 Time history: yy applied macroscale strain

A macrostrain $\epsilon^x = \begin{pmatrix} 0 & -0,75 & 0 \end{pmatrix}$ is applied using the stepping procedure described before. 20 steps are used, the tolerance used to stop the secant method iterations is set to $1 \cdot 10^{-6}$ for the modulus of the vector composed of the incremental jump between iterations on the Gauss points. In the following the resulting values for the homogenized elasticity coefficients are presented for the step 0 (no damage), step 5, step 10, step 15 and step 20 (final state) as well as the plot (Figure 4.9) of the evolution of these values:

$$\overrightarrow{S}^H_{(i=0)} = \begin{pmatrix} 7,48 \cdot 10^8 & 4,93 \cdot 10^7 & 0 \\ 4,93 \cdot 10^7 & 4,26 \cdot 10^8 & 0 \\ 0 & 0 & 4,88 \cdot 10^8 \end{pmatrix} \tag{4.14}$$

$$\overrightarrow{S}^H_{(i=5)} = \begin{pmatrix} 7,22 \cdot 10^8 & 3,90 \cdot 10^7 & 0 \\ 3,90 \cdot 10^7 & 3,48 \cdot 10^8 & 0 \\ 0 & 0 & 4,27 \cdot 10^8 \end{pmatrix} \tag{4.15}$$

$$\overrightarrow{S}^H_{(i=10)} = \begin{pmatrix} 6,90 \cdot 10^8 & 2,70 \cdot 10^7 & 0 \\ 2,70 \cdot 10^7 & 2,52 \cdot 10^8 & 0 \\ 0 & 0 & 3,42 \cdot 10^8 \end{pmatrix} \tag{4.16}$$

$$\overrightarrow{S}^H_{(i=15)} = \begin{pmatrix} 6,45 \cdot 10^8 & 2,20 \cdot 10^6 & 0 \\ 2,20 \cdot 10^6 & 2,18 \cdot 10^7 & 0 \\ 0 & 0 & 4,19 \cdot 10^7 \end{pmatrix} \tag{4.17}$$

$$\overrightarrow{S}^H_{(i=20)} = \begin{pmatrix} 6,43 \cdot 10^8 & 0 & 0 \\ 0 & 0 & 0 \\ 0 & 0 & 0 \end{pmatrix} \tag{4.18}$$

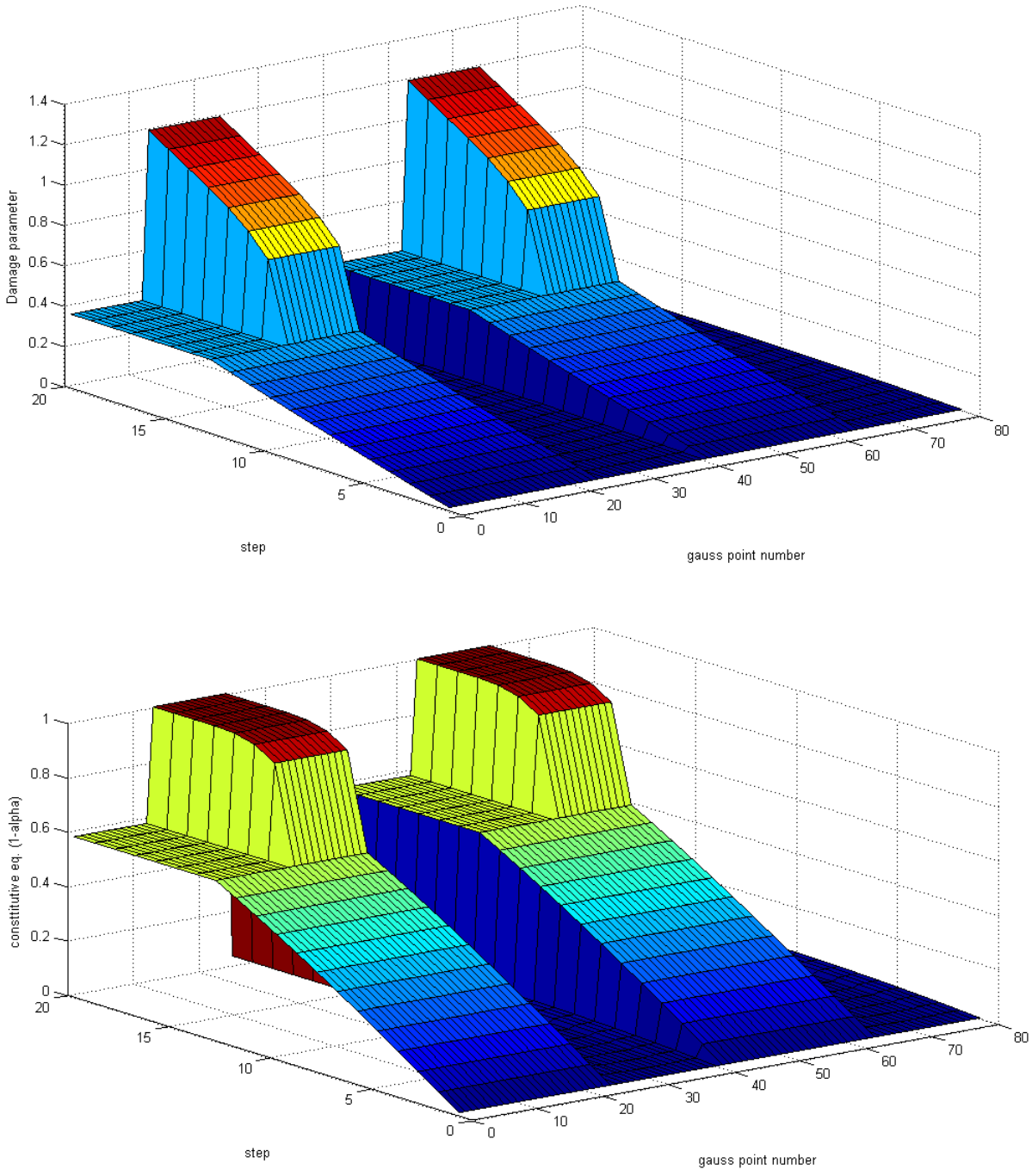

Figure 4.8: Evolution of the damage parameter and constitutive law for all the Gauss points (numbered from 0 to 80). yy applied time history.

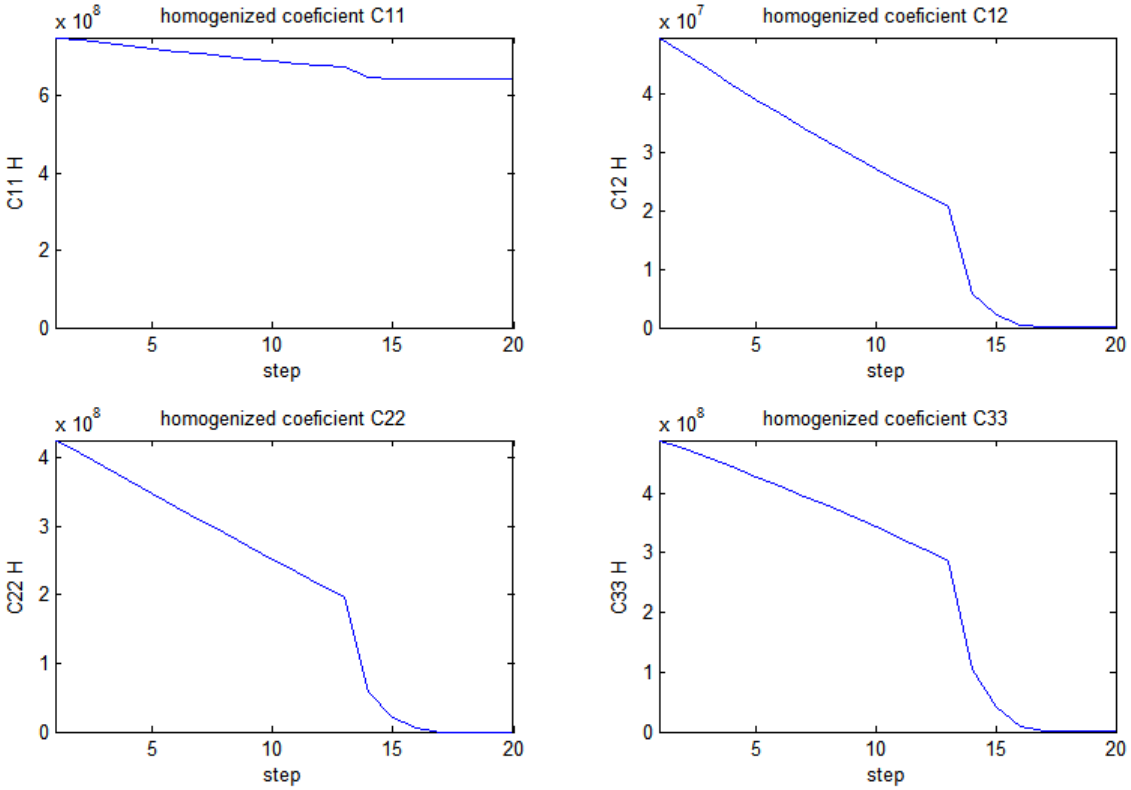

Figure 4.9: Evolution of the homogenized coefficients for the yy applied time history

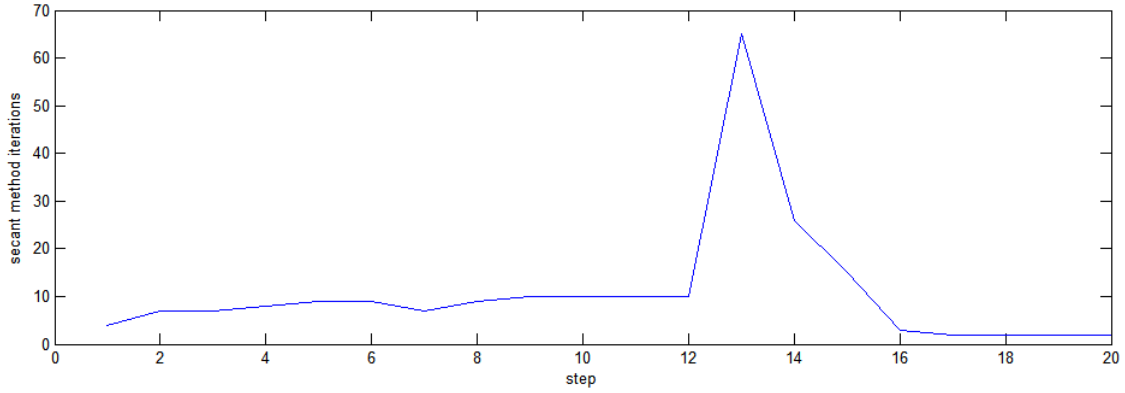

Figure 4.10: Evolution of the number of iteration in the secant method needed to reach the convergence criteria in each step. yy applied time history.

4.3.3 Time history: xy applied macroscale strain

A macrostrain $\epsilon^x = (\ 0 \quad 0 \quad -0,75\ )$ is applied using the stepping procedure described before. 20 steps are used, the tolerance used to stop the secant method iterations is set to $1 \cdot 10^{-6}$ for the modulus of the vector composed of the incremental jump between iterations on the Gauss points. In the following the resulting values for the homogenized elasticity coefficients are presented for the step 0 (no damage), step 5, step 10, step 15 and step 20 (final state)as well as the plot (Figure 4.12) of the evolution of these values:

$$\overrightarrow{S}^H_{(i=0)} = \begin{pmatrix} 7,48 \cdot 10^8 & 4,93 \cdot 10^7 & 0 \\ 4,93 \cdot 10^7 & 4,26 \cdot 10^8 & 0 \\ 0 & 0 & 4,88 \cdot 10^8 \end{pmatrix} \tag{4.19}$$

$$\overrightarrow{S}^H_{(i=5)} = \begin{pmatrix} 6,93 \cdot 10^8 & 4,07 \cdot 10^7 & 0 \\ 4,07 \cdot 10^7 & 3,79 \cdot 10^8 & 0 \\ 0 & 0 & 4,43 \cdot 10^8 \end{pmatrix} \tag{4.20}$$

$$\overrightarrow{S}^H_{(i=10)} = \begin{pmatrix} 6,19 \cdot 10^8 & 3,03 \cdot 10^7 & 0 \\ 3,03 \cdot 10^7 & 3,16 \cdot 10^8 & 0 \\ 0 & 0 & 3,82 \cdot 10^8 \end{pmatrix} \tag{4.21}$$

$$\overrightarrow{S}^H_{(i=15)} = \begin{pmatrix} 5,47 \cdot 10^8 & 2,09 \cdot 10^7 & 0 \\ 2,09 \cdot 10^7 & 2,48 \cdot 10^8 & 0 \\ 0 & 0 & 3,16 \cdot 10^8 \end{pmatrix} \tag{4.22}$$

$$\overrightarrow{S}^H_{(i=20)} = \begin{pmatrix} 4,78 \cdot 10^8 & 0 & 0 \\ 0 & 0 & 0 \\ 0 & 0 & 0 \end{pmatrix} \tag{4.23}$$

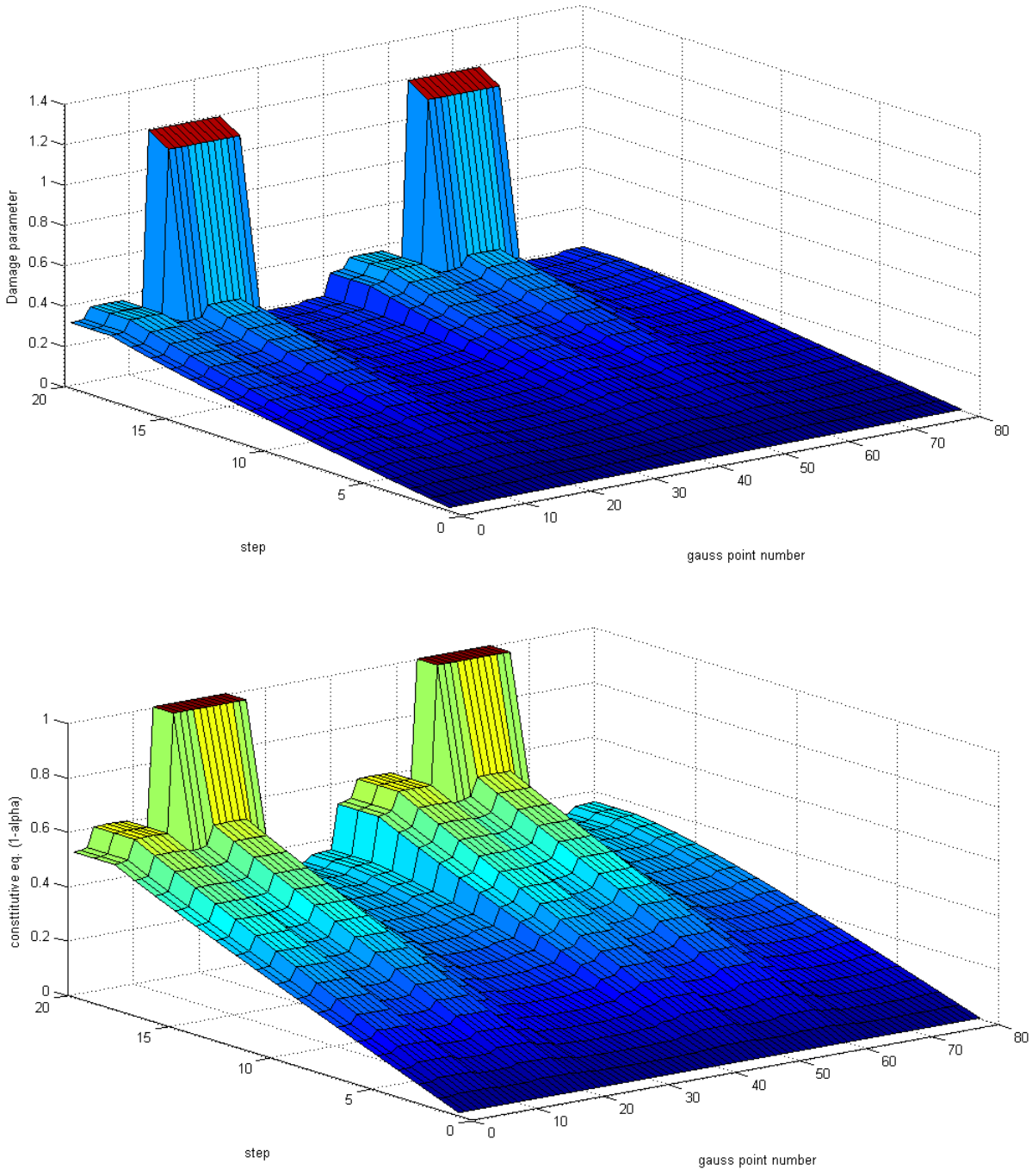

Figure 4.11: Evolution of the damage parameter and constitutive law for all the Gauss points (numbered from 0 to 80). xy applied time history.

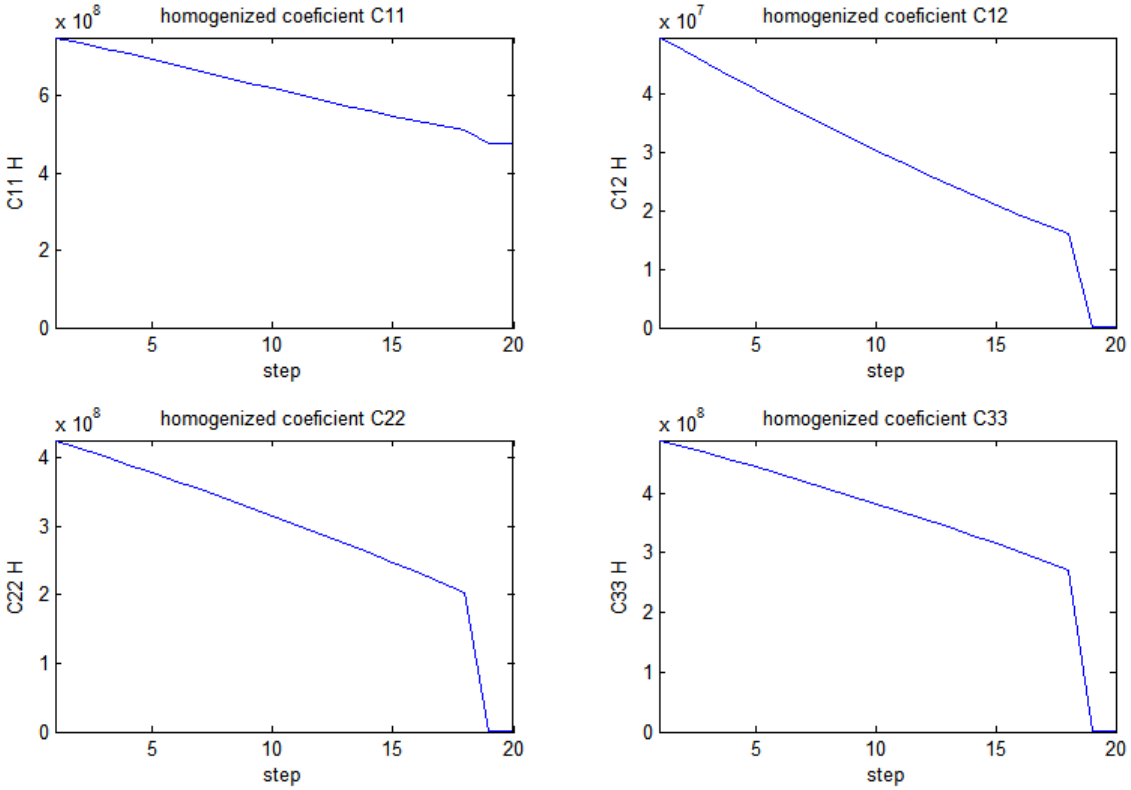

Figure 4.12: Evolution of the homogenized coefficients for the xy applied time history

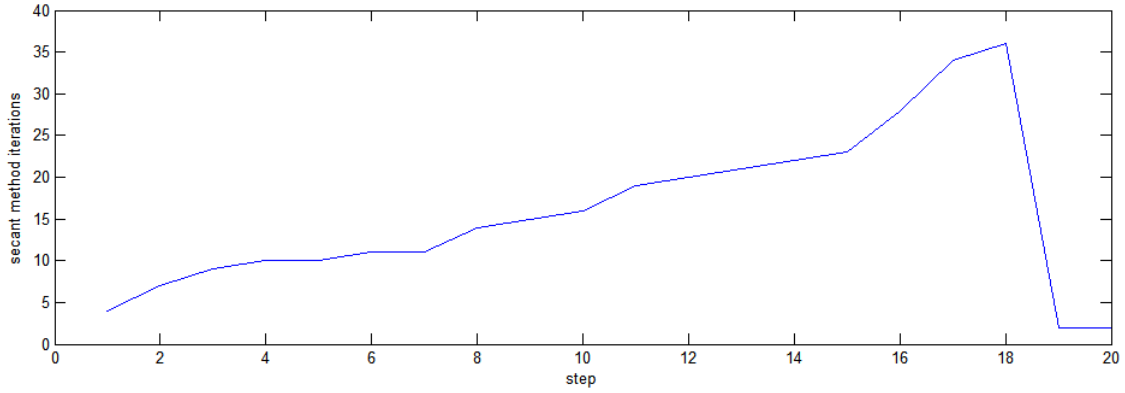

Figure 4.13: Evolution of the number of iteration in the secant method needed to reach the convergence criteria in each step.

4.3.4 Discussion of the results: homogenized coefficient evolution

From the results (Subsection 4.3.1, 4.3.2 and 4.3.3) it can be seen, as it was expected, that the damage implies a degradation of the homogenized elastic coefficients, depending on the combination of the applied macrostrains on the time history different cracks will be affected in a different manner (Figure 4.6, 4.8 and 4.11) and consequently the coefficients of the elasticity matrix will evolve depending on these macrostrains.

From the x-axis applied macroscale strain case (Figure 4.6) it can be seen that the coefficients[5] C_{11}, C_{12} and C_{33} are similarly affected but C_{22} has significantly less degradation due to the fact that the more damaged cracks are not the ones orthogonal to this axis, when the three first coefficients are almost zero, C_{22} has still more than half of the initial stiffness. Similar behavior is observed in the other time histories, even with a higher difference between the coefficients for the y-axis applied macroscale strain due to the continuity of the cracks orthogonal to this direction.

By comparing the plots of the damage and the ones of the constitutive equation, (for instance for the y-axis applied macroscale strain (Figure4.8), it can be seen that the damage parameter increases with the application of the macroscale strain even for large values, while the constitutive law reaches a plateau for values of the damage higher than 1. This is the expected behavior when the cracks are totally broken (Eq. 4.4). From these plots it can also be observed that the damage and the constitutive equation never decrease, even when some part breakes and the remaining structure releases stress. These results fulfill the definition of damage (irreversible process) (Eq.4.6).

For a very large strain, which also implies high damage, some homogenized coefficients vanish (see previous paragraph). This is due to the fact that the structure becomes very weak in some of the degrees of freedom. When this happens, any increase of strain can be applied in this degree of freedom without creating additional damage in the non broken bounds, this leads to the behavior shown (Figure 4.6) with the parameter C_{11} independent of the strain for a very large damage.

[5] For sake of simplicity, in this section Cauchy stress problem notation is changed into:
$$\begin{pmatrix}\sigma_{xx}\\ \sigma_{yy}\\ \sigma_{xy}\end{pmatrix} = \begin{pmatrix}C_{11} & C_{12} & C_{13}\\ C_{12} & C_{22} & C_{23}\\ C_{13} & C_{23} & C_{33}\end{pmatrix}\begin{pmatrix}\epsilon_{xx}\\ \epsilon_{yy}\\ \epsilon_{xy}\end{pmatrix}$$

4.4 Results: bifurcation phenomena

4.4.1 Influence of the step size

Same time-history as in (Subsection 4.3.2) is applied in this case using a 2,5 times smaller time stepping, resulting in 50 steps (figure 4.14).

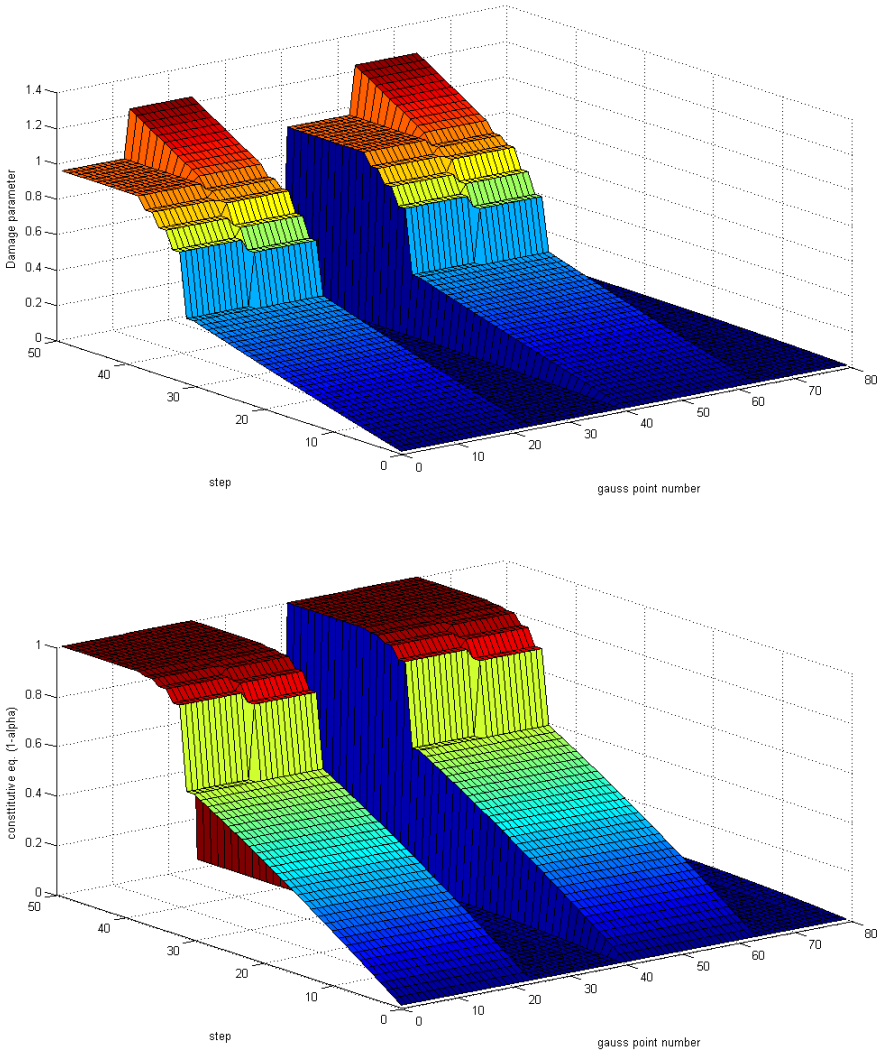

Figure 4.14: Evolution of the damage parameter and constitutive law for all the Gauss points (numbered from 0 to 80). yy applied time history. Influence of the step size.

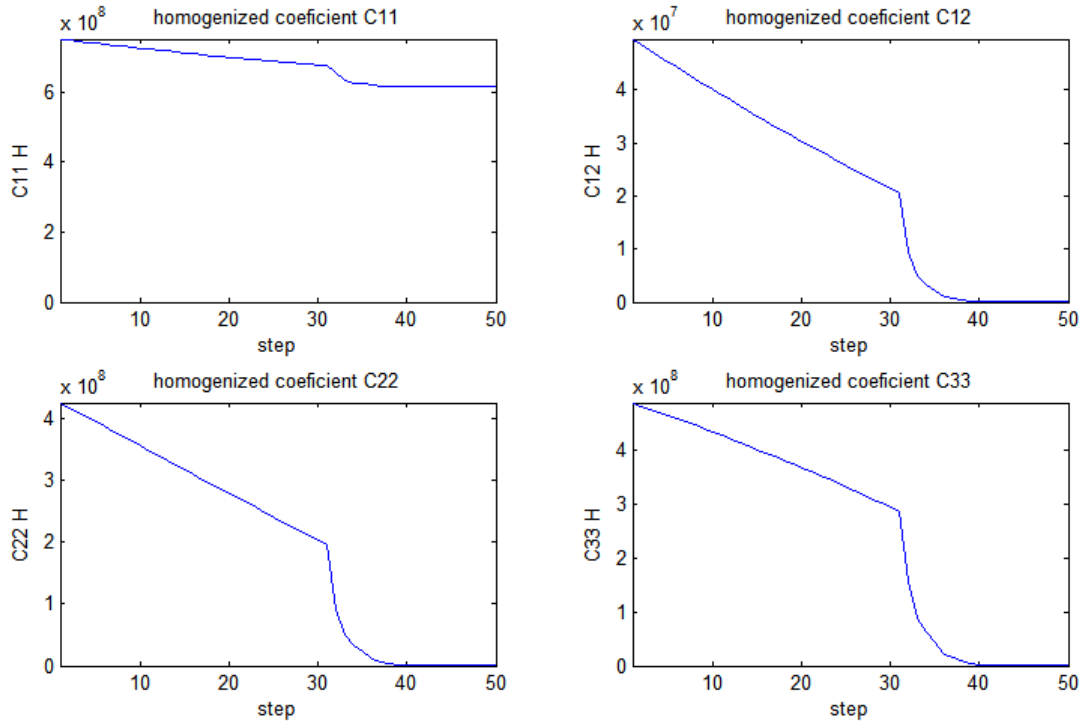

Figure 4.15: Evolution of the homogenized coefficients for the yy applied time history. Influence of the step size.

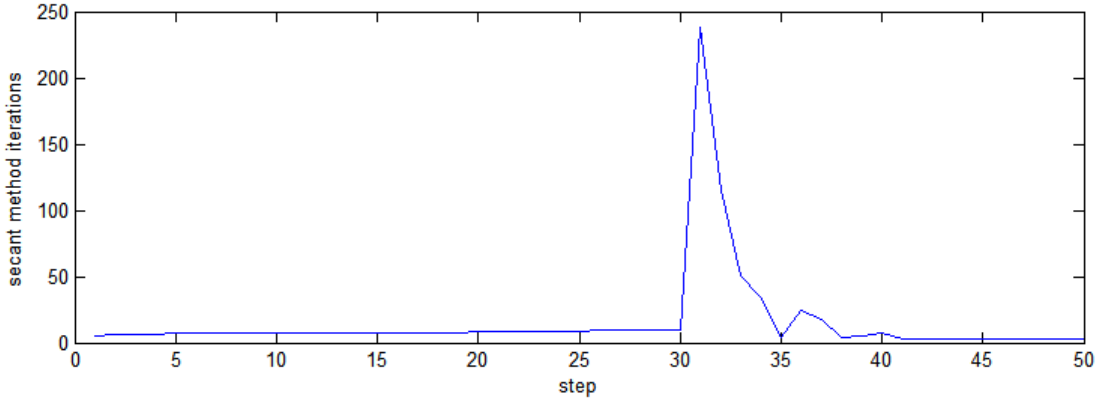

Figure 4.16: Evolution of the number of iteration in the secant method needed to reach the convergence criteria in each step. yy applied time history. Influence of the step size.

4.4.2 Influence of the damage limit

Same time-history as in (Subsection 4.3.2) is applied in this case changing the constitutive equation for one in which the cracks still have 1% of the stiffness when the damage parameter reaches 1 (Eq. 4.4). The same kind of solution than in the case with the constitutive equation (Eq. 4.3) is obtained (Figure 4.8).

4.4.3 Variation on both the stepping and constitutive law

Same time-history as in (Subsection 4.3.2) is applied in this case using a 5 times smaller time stepping, resulting in 100 steps and changing the constitutive equation for one in which the cracks still have 1% of the stiffness when the damage parameter reaches 1 (Eq. 4.4) (Figure 4.17).

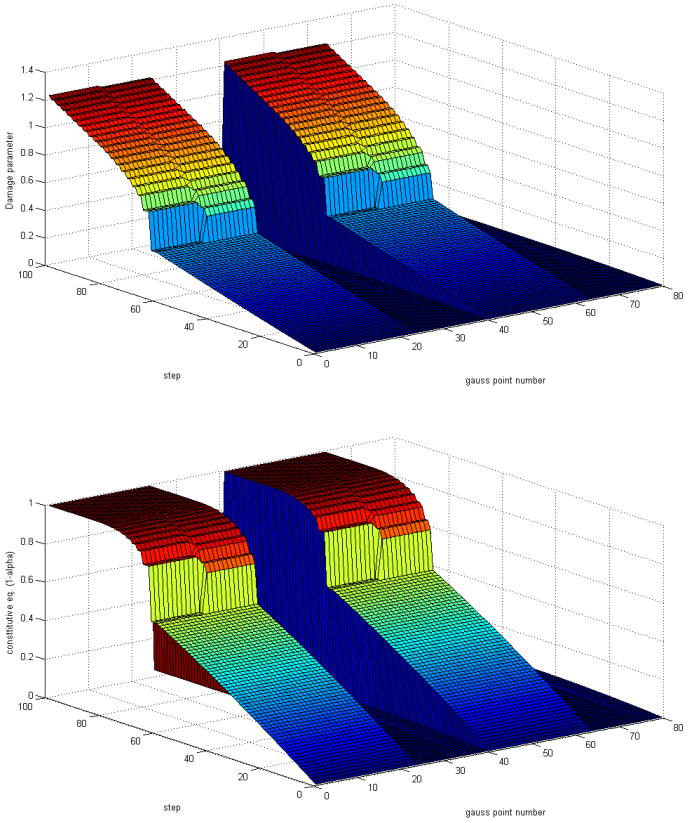

Figure 4.17: Evolution of the damage parameter and constitutive law for all the Gauss points (numbered from 0 to 80). yy applied time history. Variation on both the stepping and the constitutive law.

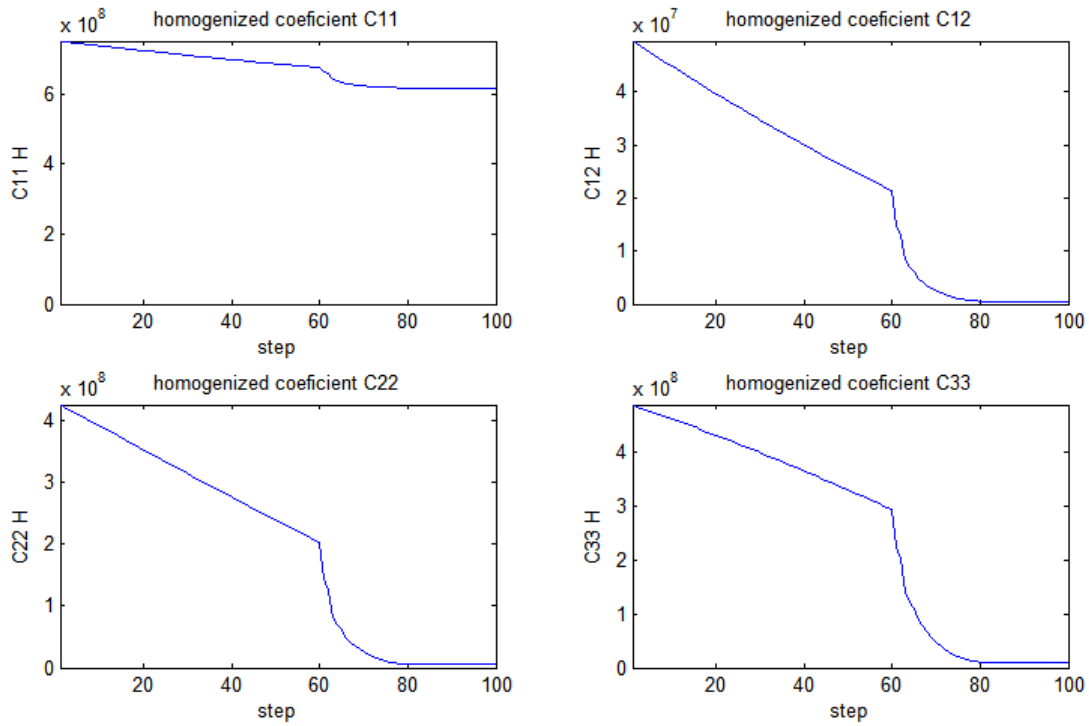

Figure 4.18: Evolution of the homogenized coefficients for the yy applied time history. Variation of both the stepping and the constitutive law.

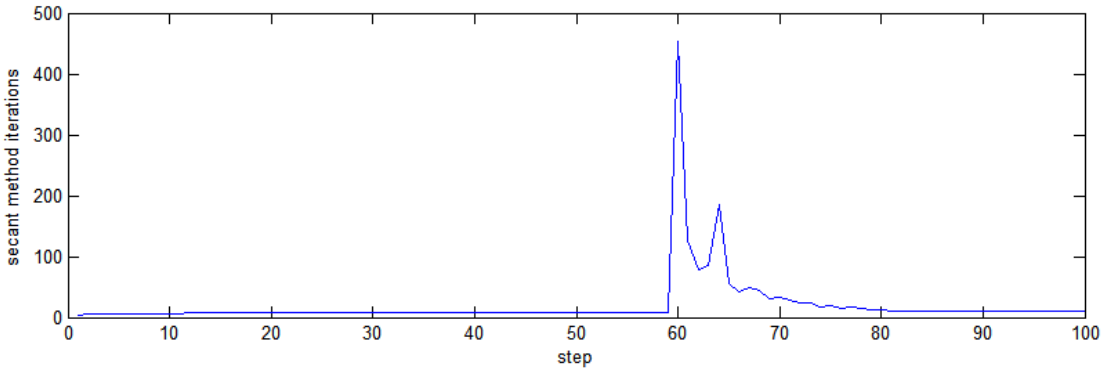

Figure 4.19: Evolution of the number of iteration in the secant method needed to reach the convergence criteria in each step. yy applied time history. Variation on both the stepping and the constitutive law.

4.4.4 Comparison homogenized coefficients evolution with different time-step size

The same time-history as in (Subsection 4.3.1) (xx applied macrostrain) is applied in this case together with the cases using 5 and 25 times smaller time stepping, resulting in 100 and 500 steps (Figure 4.20 and 4.21).

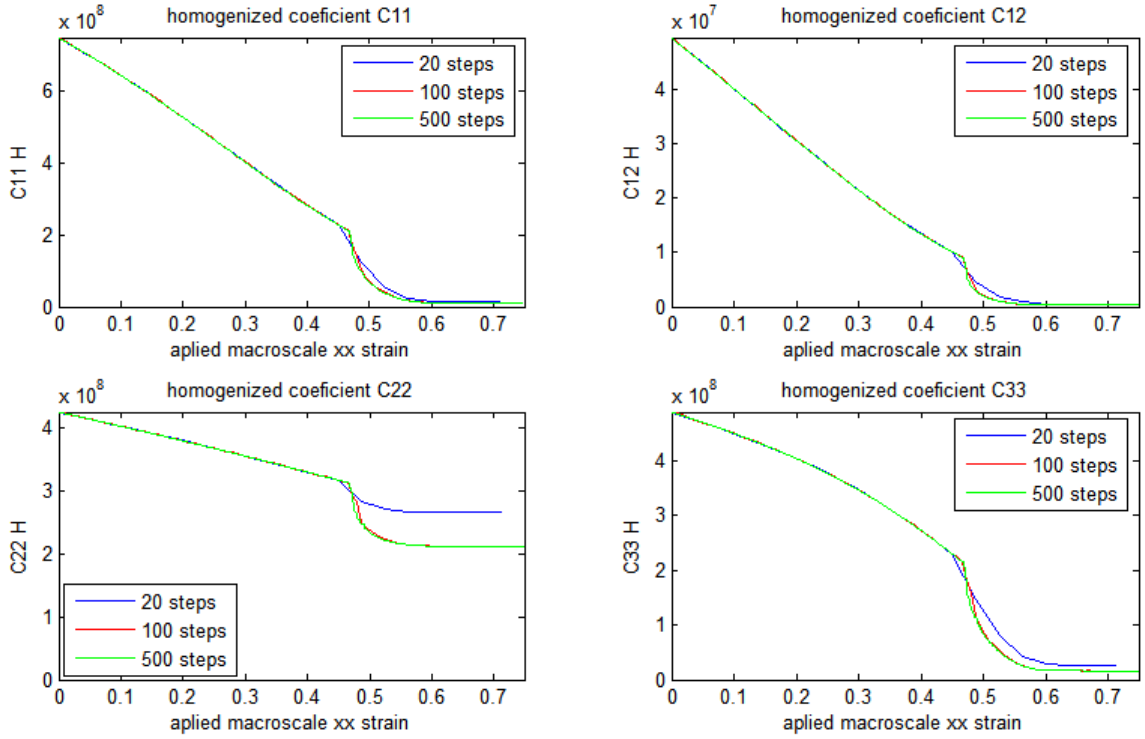

Figure 4.20: Evolution of the homogenized coefficients for the xx applied time history for a three different time-history step sizes: 20 steps, 100 steps and 500 steps.

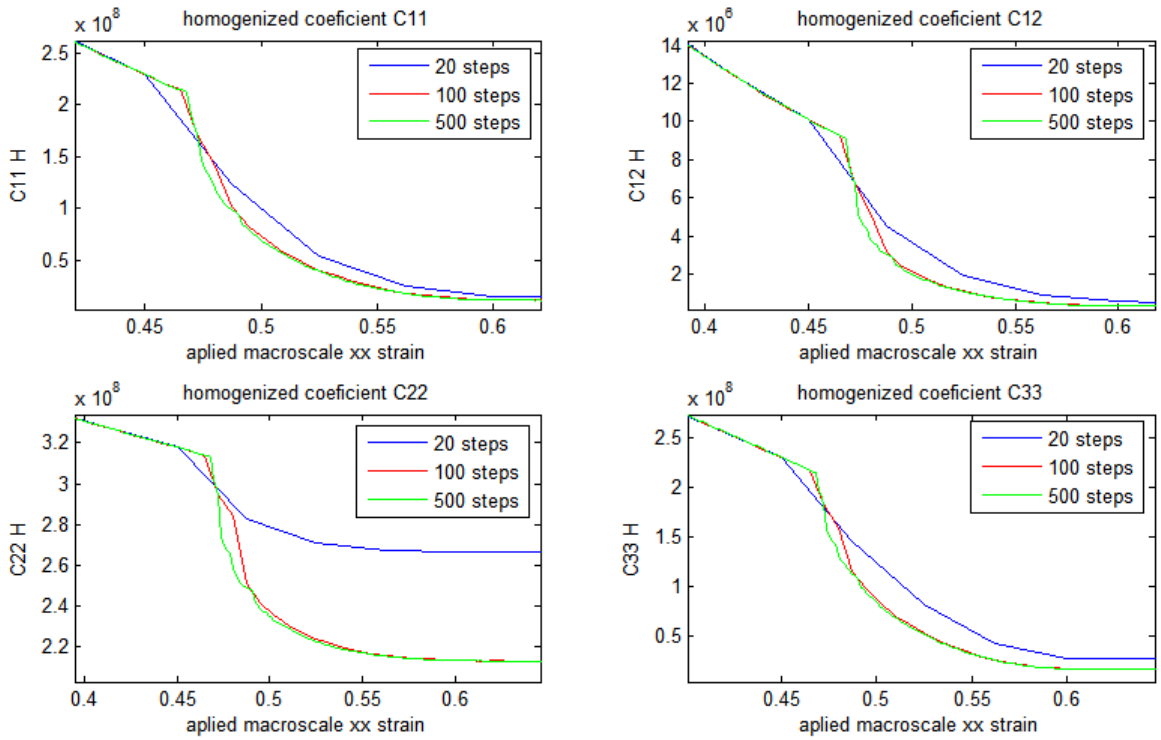

Figure 4.21: Evolution of the homogenized coefficients for the xx applied time history for a three different time-history step sizes: 20 steps, 100 steps and 500 steps. Detail of the sudden degradation of the coefficients.

4.4.5 Discussion of the results: bifurcation phenomena[6]

Although this was not one of the targets of this project bifurcation phenomena will be discussed since they can be observed in the results. Bifurcation occurs when more than one possible result coexist. When bifurcation occurs a small change of the parameters of the model produces a sudden change in the solution. This can be observed in the results (Figure 4.6, 4.8 and 4.11) when the elastic coefficients drop quickly after a given iteration, this happens when some cracks increase the opening to a very high value but at the same time other cracks close because the release of stress produced by the opening of the firsts. A priory it is not known which cracks are going to open and which ones to close, and this result can change randomly (Figure 4.22) depending on the small change on the parameters already commented. Because of the symmetries of the REV, the two possible solutions for this bifurcation give as a result the same elasticity coefficients. From the numerical point of view the existence of two different possible solutions can make the iterative methods slower or not convergent due to the fact that iterative methods can jump from one to the other solutions without reaching any convergence (Figure 4.19).

For the particular case of this project, after the bifurcation takes place, the elastic coefficients are degraded very quickly to values near zero, this makes the system matrix of the FEM model a near singular matrix[7]. As it is known, the solution of a system with a near singular matrix will lead to inaccurate results (Figure 4.22). To deal with this, and in order to observe the different solutions after the bifurcation, the time-history must be stopped immediately after the bifurcation happens (Figure 4.23).

In order to study the bifurcation, further simulations are carried out (Subsection 4.4.1, 4.4.2 and 4.4.3). By decreasing the size of the time-history steps, it can be observed that the bifurcation doesn't take place suddenly in one iteration but, in several bifurcations along several steps (Figure 4.15) until the damage value reaches 1, after that, the bifurcation splits clearly into two solutions. In order to avoid the instabilities that may be caused by the zero value of the constitutive equation (Eq. 4.3) a modified equation with a remaining 1% of stiffness for a totally broken crack is introduced (Eq. 4.4) leading to bifurcation results again. Another simulation combining a smaller time-history stepping and the modified constitutive law is presented (Figure 4.17) showing bifurcation in several steps, but without two clearly differentiated solutions like the ones in previous simulations.

From the previous results it can be said that the modification of the constitutive equation has not a significant effect on the bifurcation triggering, while the change of the step size can produce a qualitative change on the evolution of the problem (Figure 4.20 and 4.21), but further research should be done in order to understand the implication of the different parameters.

[6] This phenomena can also be observed in experimental results named as strain localization.

[7] Or what is the same, the difference between the minimum and the maximum eigenvalues of the matrix is very large. Also due to the fact that penalization method is used both for the periodicity conditions and to avoid the kinematic indetermination, this will provide the maximum eigenvalue, while the most damaged cracks will provide the minimum.

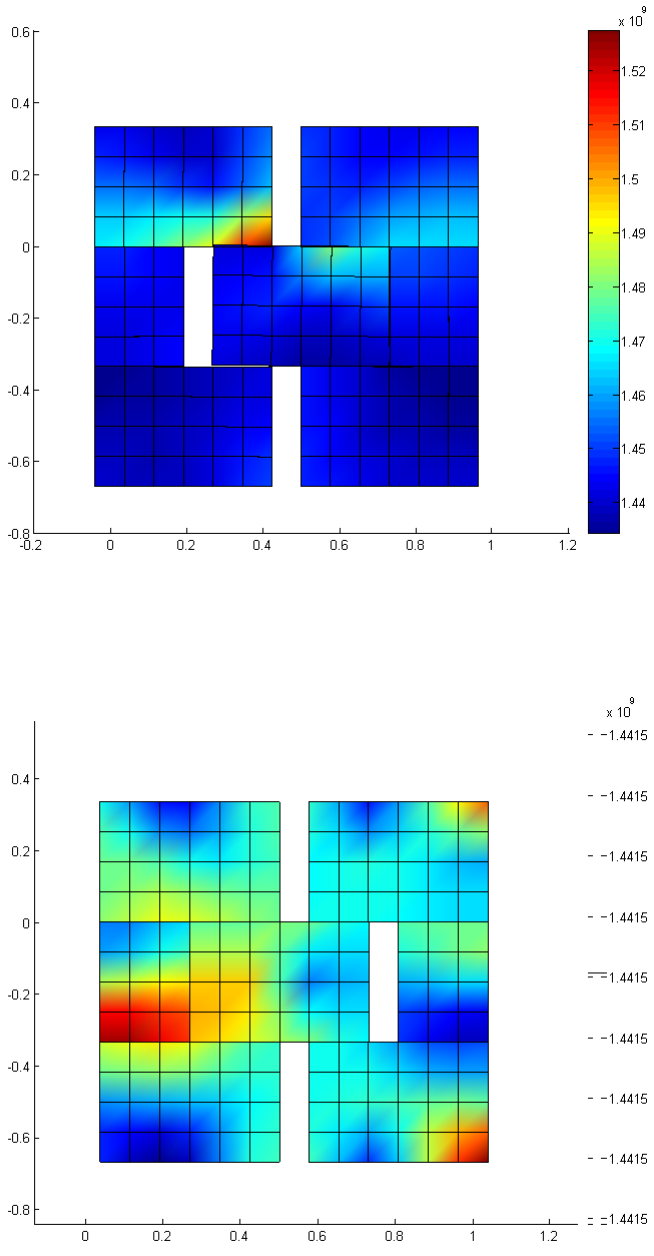

Figure 4.22: Result for the last step of the calculation for a time history macroscale strain (-0,75 0 0), time history applied in 20 and 22 steps. It can be seen that the final results has two possible configurations. Because the system is near to be a mechanism the solution is not accurate.

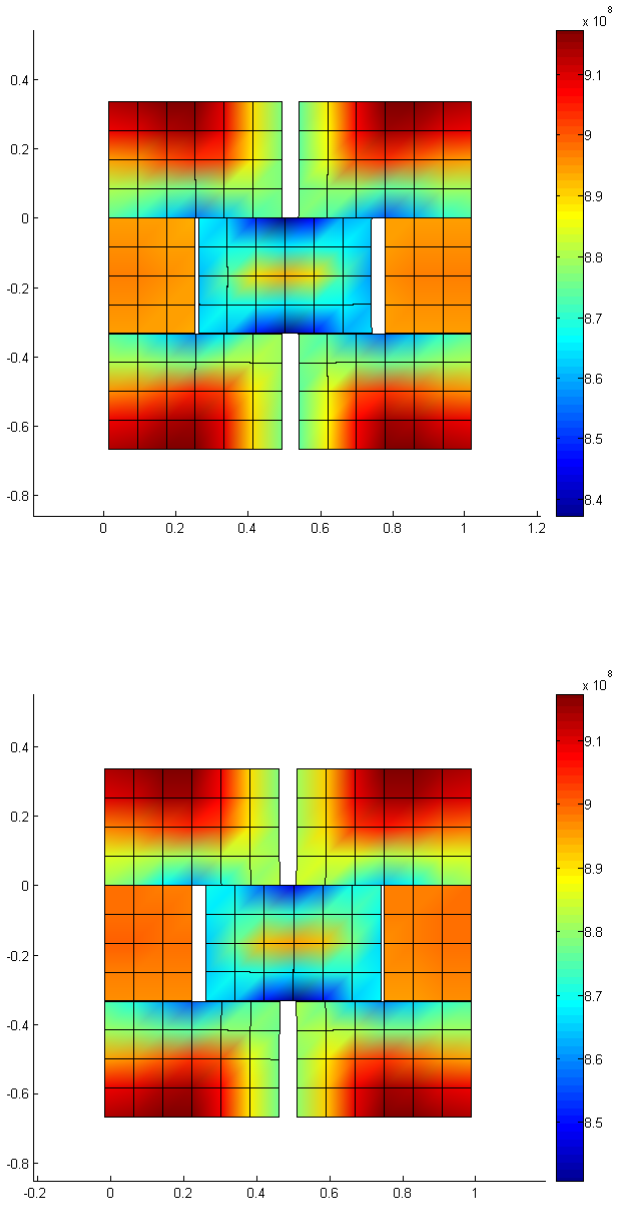

Figure 4.23: Result for the last step of the calculation for a time history macroscale strain (-0,49 0 0) time history applied in 10 and 11 steps. It can be seen that the final result has two possible configurations.

Chapter 5

Conclusions

This work has started with the numerical resolution of an homogenized problem in a REV of a cracked poroelastic medium. The numerical results of the mechanical problem show an heterogeneous solution due to the coupling between porous media and cracks, while for the hydraulic problem the solution is homogenous, therefore no numerical tools are needed for the resolution of the hydraulic problem. From the solution of those problems the homogenized coefficients can be obtained. The coefficients introduced in the microscale are isotropic, however in the macroscale the problem becomes orthotropic due to the crack geometry used in the REV. In a second part of the work damage on the cracks is considered, damage depends on the opening of the cracks and implies a degradation of the coefficients in the microscale problem. Using numerical methods for nonlinear problems an evolution of the homogenized coefficients is obtained for a time-history of applied strain. In some point of the time-history for a high enough values of damage a sudden degradation is observed together with bifurcation phenomena.

Chapter 6

Perspectives

Because the solution presents bifurcation phenomena for large damage values, and this is constricted by the size of the REV, a further research concerning the influence of the REV size to the evolution of the homogenized coefficients can be done. Since a bigger REV means a lower constriction to the possible failure mechanisms a lower strain value for the sudden degradation triggering is expected for increasing sizes of REV.

The obtained homogenized coefficients can be used in any real scale geomechanics or engineering problems, or in a more general sense, any problem of material science concerning cracked poroelastic media with deformation and fluid flow. Therefore, further research including the study of the microscale configuration and the calibration of the microscale coefficients with real materials can be done.

Bibliography

[1] D. Caillerie. *Homogenization of periodic media,* Course, Grenoble INP - UJF - CNRS, 2009.

[2] F. Marinelli. *Comportement couplé des géomatériaux: deus approches de módelisation numérique,* Phd thesis, Laboratoire 3S-R, Ecole Doctorale IMEP2, 2013.

[3] E. Papachristos. *Homogenization of a Cracked Poroelastic Medium*, Master thesis, UJF - Grenoble INP, 2012.

Appendix A
Variational expressions for the finite element implementation

Poroelasticity problem grains

-(solid.Sl11*test(solid.el11) +2*solid.Sl12*test(solid.el12) +2*solid.Sl13*test(solid.el13)
+solid.Sl22*test(solid.el22)+ 2*solid.Sl23*test(solid.el23) +solid.Sl33*test(solid.el33)
+a*(solid.D11*test(solid.el11) +solid.D12*test(solid.el22)) +2*b*solid.D44*test(solid.el12)
+c*(solid.D12*test(solid.el11) +solid.D22*test(solid.el22)) +dp*bco.po*(-test(solid.el11)
-test(solid.el22)-test(solid.el33)))*solid.d

Poroelasticity problem cracks

-1.0E12*solid.d*(solid.uspring1_tel1* (sys1.Tdef11*test(up(u)-down(u))
+sys1.Tdef12*test(up(v)-down(v))) +solid.uspring2_tel1* (sys1.Tdef21*test(up(u)
-down(u)) +sys1.Tdef22* test(up(v)-down(v)))) +bco.crt*d* (sys1.Tdef11*test(up(u)
-down(u)) +sys1.Tdef12* test(up(v)-down(v)))+bco.crn*d* (sys1.Tdef21*test(up(u)
-down(u)) +sys1.Tdef22* test(up(v)-down(v)))

Thermal/hydraulic problem grains

-((ht.k_effxx*(Tx+c) +ht.k_effxy*(Ty+d))*test(Tx)
+(ht.k_effyx*(Tx+c) +ht.k_effyy*(Ty+d))*test(Ty))*ht.ds a*(ht.k_effxx*(Tx+a))
+b*(ht.k_effyy*(Ty+b))

Thermal/hydraulic problem cracks

-((ht.k_effxx*(TTx+a) +ht.k_effxy*TTy)*test(TTx)
+(ht.k_effyx*TTx+ht.k_effyy*(TTy+b))*test(TTy))*ht.ds